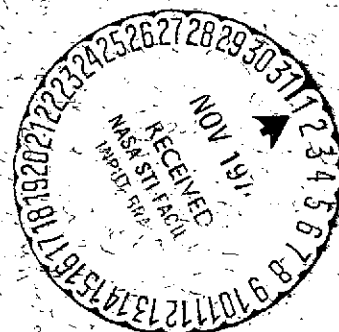X-662-74-304
PREPRINT

NASA TM X- 70761

HIGH ENERGY GAMMA RAY RESULTS FROM THE SECOND SMALL ASTRONOMY SATELLITE

C. E. FICHTEL
R. C. HARTMAN
D. A. KNIFFEN
D. J. THOMPSON
G. F. BIGNAMI
H. ÖGELMAN
M. F. ÖZEL
T. TÜMER

NOV 19
RECEIVED
NASA STI FACIL
INPUT BRA

OCTOBER 1974

GSFC

—— GODDARD SPACE FLIGHT CENTER ——
GREENBELT, MARYLAND

High Energy Gamma Ray Results
From the Second Small Astronomy Satellite

C. E. Fichtel, R. C. Hartman, D. A. Kniffen,
D. J. Thompson, G. F. Bignami*

NASA/Goddard Space Flight Center
Greenbelt, Maryland 20771

H. Ögelman, M. F. Özel, T. Tümer

Middle East Technical University
Ankara, Turkey

ABSTRACT

A high energy ($>$ 35 MeV) gamma ray telescope employing a thirty-two
level magnetic core spark chamber system was flown on the second Small
Astronomy Satellite (SAS-2). The high energy galactic gamma radiation is
observed to dominate over the general diffuse radiation along the entire
galactic plane and is seen to be most pronounced in a region from ℓ^{II} = 335°
to ℓ^{II} = 40°. When examined in detail the longitudinal and latitudinal
distribution seem generally correlated with galactic structural features,
and particularly with arm segments. On the basis principally of its
angular distribution and magnitude, the general high energy gamma
radiation from the galactic plane seems to be explained best as resulting
primarily from cosmic ray interactions with interstellar matter. From the
study of six different regions of the sky with $\mid b^{II} \mid$ > 30°, there appears
to be a uniform celestial gamma radiation, as suggested by earlier results,
especially Kraushaar et al. (1972). Over the energy range from about
35 MeV to 170 MeV, the differential spectrum has the form

*ESRO Postdoctoral Fellow on leave from LFCTR, Istituto di Fisica dell'
Universitā di Milano, Italy

$$\frac{dJ}{dE} = (2.7 \pm 0.5) \; \left(\frac{E}{100}\right)^{-2.4 \pm 0.2} \; \frac{\text{gamma rays}}{\text{cm}^2 \text{ sr sec MeV}}$$

where E is expressed in MeV. If the apparent flattening of the spectrum in the 0.6 to 10 MeV region observed in other experiments is verified, the high energy results reported here when combined with the lower energy data suggest a cosmological origin for this radiation. Three low energy gamma ray bursts were observed in the large SAS-2 anticoincidence scintillator in the period from November 19, 1972 to June 8, 1973, perhaps a surprisingly small number in view of the high sensitivity of the anticoincidence scintillator. In addition to the general galactic emission, high energy gamma radiation was seen from the Crab nebula (a significant fraction of which is pulsed at the radio pulsar frequency), Vela-X (a supernova remnant whose high energy gamma radiation possibly provides the first direct experimental evidence associating cosmic rays with supernovae), the general region ($15° < b^{II} < 30°$, $340° < \ell^{II} < 20°$), and a region a few degrees north of the galactic plane around 190° to 195° in ℓ^{II}. Several upper limits to high energy gamma ray fluxes were also set, including among others, above 100 MeV: $1.0 \cdot 10^{-6}$ for the Small Magellanic Cloud, $9.5 \cdot 10^{-7}$ for Sco X-1, $2.5 \cdot 10^{-6}$ for 3C120, $1.0 \cdot 10^{-6}$ for M-87, and $1.1 \cdot 10^{-6}$ for Cas A in units of photons (E>100 MeV)/ (cm^2 sec).

Subject headings: Gamma rays -- galactic structure -- celestial diffuse radiation -- gamma ray bursts -- galactic cosmic rays -- Supernova remnants -- pulsar -- Vela-X -- Crab nebula

I. INTRODUCTION

Although high energy gamma ray astronomy has long been known to hold potentially great rewards because of its ability to reveal the dynamic, high energy processes in our galaxy and the universe, its development has been slow and difficult, primarily because of the low intensity of celestial gamma rays both in absolute terms and relative to the cosmic rays. Whereas some gamma radiation presumably arises simply from high energy extensions of the same mechanisms responsible for x-rays (bremsstrahlung, the inverse Compton effect, and magneto bremsstrahlung), other components probably have origins unique to the γ-ray region. There are, for example, the gamma rays produced by the decay of neutral pions formed in the collision of energetic cosmic ray nucleons with the interstellar nuclei and by nucleon-antinucleon annihilation.

The first certain detection of celestial gamma rays came from a satellite experiment flown on OSO-3. With this detector, Kraushaar et al. (1972) observed the emission of gamma rays with energies above 50 MeV from the galactic disk with a peak intensity toward the galactic center. However, the limited spectral and spatial resolution of this pioneering experiment left many questions unanswered. Four other early satellite high energy gamma experiments were those on COSMOS-208 (Bratolyubova et al., 1971), COSMOS-264 (Galper et al., 1973), OGO-5 (Hutchinson et al., 1971), and OSO-3 (Valentine et al., 1971). During the last decade, there have also been numerous attempts to detect high energy gamma radiation with balloon-borne experiments, but these have been seriously hampered by the high level of atmospheric gamma rays due to cosmic ray interactions in the atmosphere. The results of these

experiments, largely upper limits, will be mentioned in this article where they are relevant.

The experiment to be described here is a picture-type high energy (> 35 MeV) gamma ray telescope using thirty-two magnetic core spark chambers and flown on the second NASA Small Astronomy Satellite (SAS-2). It has the advantages of providing a wide field of view (full width half maximum angle of 35°), but still permitting a few degrees angular resolution for individual gamma rays and providing positive identification of the gamma rays, as well as an estimate of their energy. Results to be reported here from the SAS-2 satellite fall into four subject areas: the relatively intense component from the galactic plane with its hard energy spectrum; the diffuse, apparently extragalactic radiation; low energy gamma ray bursts; and localized sources. A discussion of each of these will follow the experiment description given in the next section.

II. THE EXPERIMENT

A. Gamma Ray Telescope Description

A schematic diagram of the gamma ray telescope flown on SAS-2 is shown in figure 1. The spark chamber assembly consists of 16 magnetic core spark chamber modules above a set of four central plastic scintillators and another 16 modules below these scintillators. Thin tungsten plates, 0.03 radiation length thick, are interleaved between the spark chamber modules, which have an active area of approximately 640 cm^2. The large number of thin tungsten plates and spark chambers serve a dual purpose: first, to provide material for the gamma ray to be converted into an electron pair which can then be clearly identified

and from which the arrival direction of the gamma ray can be determined; and secondly, to provide a means of determining the energy of the electrons in the pair by measuring their Coulomb scattering. The array of four plastic scintillator tiles in the center of the spark chamber telescope constitute the first elements (B_i) of four independent counter coincidence systems, of which the lower element is a directional Cerenkov detector (C_i). A single-piece plastic scintillator dome (A) surrounds the spark chamber system except at the bottom of the experiment, as shown in Figure 1.

A gamma ray entering the top of the telescope converts into an electron pair in one of the 15 tungsten plates in the upper half of the spark chamber with a known efficiency, to be discussed later in this section. If either electron passes through at least one of the four counter coincidence systems, the spark chambers are fired provided there is no pulse from the anticoincidence scintillator dome, and the readout of the set magnetic cores is initiated. The purpose of the scintillator dome is to discriminate against the very large number of charged particles which pass through the experiment.

The use of this relatively complex detector system was dictated by two primary considerations. First, the flux of charged cosmic rays is from three to four orders of magnitude larger than the gamma ray fluxes to be observed, and therefore it is essential to identify uniquely the gamma ray events through a pictorial presentation so that they may be separated from other events which might meet coincidence requirements. Second, the telescope should provide an angular resolution of a few degrees for individual gamma rays while at the same time having a large acceptance solid angle.

A digitized spark chamber "picture" of a gamma ray-induced electron pair is shown in figure 2.

Each of the four plastic scintillator tiles is 12.7 cm x 12.7 cm x 0.5 cm thick, and is coupled by an adiabatic light-pipe to a photomultiplier tube outside the spark chamber gas volume. Each of the acrylic plastic Cerenkov radiators, 2.5 cm deep, is viewed from below by a 12.5 cm photomultiplier tube. The top of each radiator is coated black to absorb the Cerenkov light generated by upward moving charged particles, thereby discriminating against relativistic particles entering from below, but not traveling as far as the anticoincidence dome.

As mentioned above, the digital spark chambers utilize the ferrite core readout technique. Each spark chamber module contains two parallel planes of wires, with the wires in one plane orthogonal to those in the other plane. Each wire passes through a small memory core at the edge of the module. The 200 wires in each plane are spaced 0.127 cm apart, providing an active area of 25.4 x 25.4 cm^2. The spark chamber module to spark chamber module height spacing is 1.14 cm, and the entire spark chamber stack has a height of 38 cm. When collecting celestial gamma ray data in orbit, the experiment percentage live time is between 85% and 90%, with the remaining time being used to readout and record the core locations.

The anticoincidence dome is made from 1.5 cm thick plastic scintillator. It is viewed from the bottom by eight equally-spaced 3.8 cm photomultipliers. Its inefficiency for detection of minimum ionizing singly-charged particles, entering within the solid angle of

the coincidence telescopes, is less than 10^{-5}.

Within every 3 second period, counting rates of the B_i and C_i counters, coincidence counts of each of the four coincidence systems (B_i and C_i), and the "neutral" counts ($\overline{AB_i}C_i$) are recorded. The counting rate of the anticoincidence dome is recorded every 0.77 seconds.

The energy threshold is about 30 MeV. The energy of the gamma ray can be measured up to about 200 MeV, and the integral flux above 200 MeV can be determined. The complete experiment weighs 85 kg. and requires 10 watts of electrical power. A more complete discussion of the SAS-2 gamma ray telescope is given by Derdeyn et al. (1972).

B. Satellite Characteristics

The gamma ray telescope is mounted at its base to the SAS-2 spacecraft, which provides electrical power, commands, data recording, telemetry, attitude control, and aspect sensing. SAS-2 is spin stabilized with magnetic torquing to allow pointing to any region of the sky. Although the spin rate is only 0.1 to 0.2 rpm, a momentum wheel reduces the drift rate to a few degrees per day, or less. The spacecraft aspect is monitored by two separate sets of sensors. A digital solar aspect detector and a 3-axis set of magnetometers together are capable of providing aspect accuracy of about 0.3°. Star sensor data can refine the accuracy to about 0.2°. All experiment data, as well as spacecraft housekeeping data, are stored on one of the two identical tape recorders, at a rate of 1 kilobit per second, of which approximately 2/3 is devoted to spark chamber data. A more detailed description of the SAS-2 spacecraft has been given by Townsend (1969).

The low fluxes involved in the study of celestial gamma radiation

make it desirable that the collection of useful satellite data be as complete as possible. These considerations led to the choice of a low earth equatorial orbit (2° inclination with an apogee of 610 km and a perigee of 440 km), and an orbital period of 95 minutes.

The observation program was planned to provide an exposure to the entire sky within one year of operation, with early emphasis being placed on the galactic plane. Some early exposures to regions of intermediate and high galactic latitudes were included for study of possible discrete sources and of the diffuse gamma radiation. The time required for magnetic torquing from one direction to another was typically several hours. However, because of the low intensity of celestial gamma rays, with the given opening angle, the optimum time for viewing one region of the sky was about one week; therefore, this torquing period did not impose a serious limitation.

The satellite was launched on November 15, 1972, and the experiment was activated on November 19, 1972. On June 8, 1973, a failure in the input portion of the low voltage power supply ended the collection of data from SAS-2. At that time approximately 55% of the sky had been examined, including most of the galactic plane as shown in figure 3.

The two tape recorders were used on alternate orbits. At the time of the acquisition of the spacecraft signal at the Quito, Ecuador ground station, the alternate recorder was switched on and the active recorder was placed in the playback mode, transmitting data from the previous orbit to the ground station. At 20 kilobits per second, the playback time was about 5 minutes. During the time remaining before loss of signal, real time data at 1 kilobit per sec. were recorded at the ground station

along with station time, which had an absolute accuracy of better than 0.1 milliseconds. This information provides an absolute time reference for the spacecraft clock, and together with other considerations permits determination of the arrival times of individual gamma rays to an accuracy of $\pm$ 1 millisecond, the principal undertainty resulting from the spacecraft clock and the experiment event timing signal.

The results to be reported here include data from the entire portion of the galactic plane that was viewed by SAS-2 together with those portions of the sky not on the galactic plane viewed during the first fifteen weeks of operation.

C. Data Reduction

1. General

As discussed in Section IIB, there was very nearly full data collection during the active life of SAS-2. All data from the Quito ground station were accumulated at GSFC's Information Processing Division where quality checks were made and a relationship established between universal time and the spacecraft clock, based on the correlation with the ground station clock during the real time portion of the data transmission corrected for propagation delay. The resulting information was supplied in digital form on an experimenter tape containing all experiment and spacecraft data annotated with a corrected time base accurate to ± 1 millisecond. These data were combined with orbit and attitude data analyzed separately to provide a master "encyclopedia" of data with which to perform experiment analysis. The encyclopedia was then used both as the basis for individual

gamma ray event analysis and for calculating the exposure parameters
for each region of the sky.

   2. Gamma Ray Events

   The first step in the reduction of the experiment data is the
selection of unambiguous gamma ray events from all those events which
have satisfied the trigger logic of the spark chamber. The creation
of a positron-negatron pair is a unique interaction leading to a
distinctive picture. The events which are eliminated fall largely into
two categories. The first of these includes all events which originate
in the detector walls rather than in the conversion plates. While some
such events may be of gamma ray origin, their interpretation would be
ambiguous. The majority of the remaining events fall into the second
category--single track events. These events are largely electrons
entering through the bottom of the detector (resulting from the fact
that the directional Cerenkov counter is not absolute in rejecting
backward moving particles). Some of these events may be Compton elec-
trons or very high energy unresolved pairs, but, since these cannot be
unambiguously separated from the others, all single track events are
rejected, and the efficiency is determined on the basis of those gamma
rays which create clearly defined pairs.

   The selection of events is based on a set of rules designed to
insure that no ambiguities will be introduced into the measured results
due to the acceptance of events not associated with gamma rays. Both
the calibration and flight data were analyzed using the same criteria
to maintain consistency of interpretation and correctly determine effec-
tive efficiencies. These rules can be summarized as follows:

(a) Data intervals are selected in which the detector axis
   was within 90° of the vertical from the earth.

(b) Only events which show two tracks with a common point
   of origin in the top half of the spark chamber tele-
   scope are selected; that is, those appearing as an
   inverted "Y" or "V" in at least one of the two ortho-
   gonal views. To be considered as a track, there must
   be sparks in at least three decks.

(c) The projected opening angle of the pair must be less
   than 35° in each view.

(d) Events appearing to originate in the walls of the
   chamber are rejected.

(e) Any event showing a spark in the top deck of the spark
   chamber is rejected. This eliminates those gamma rays
   which undergo pair production in the small amount of
   matter between the anticoincidence dome and the top
   grid, as well as the very rare charged particle which
   leaks through the anticoincidence dome.

Those events which are selected by this set of criteria are edited
on an interactive graphics display device as necessary. This procedure
identifies the sparks associated with the positron-negatron pair and
eliminates spurious sparks. The events are then automatically proces-
sed to determine energy and direction of each detected gamma ray.

Energy calculations are based on the multiple scattering of the
pair electrons in the tungsten plates. The formalization for this

analysis has been discussed in detail previously, but has been extended

for this work to include uneven cell size as encountered when an electron

does not have set core locations in some decks because of the finite

spark chamber efficiency. The mathematical details of this development

are presented in the Appendix. The quantitative accuracy has been

verified by detailed calibrations, which will be discussed in the

following section.

Gamma ray arrival directions are based on a weighted bisector

method which weights the estimated direction toward the higher energy

electron (Fichtel et al.,1972). From the arrival direction in tele-

scope coordinates, the attitude data are used to transform the apparent

direction of arrival of the ambient photon into any selected celestial

coordinate system. The accuracy of the directional determination will

be discussed in section 3. In the subsequent analysis only gamma rays

whose arrival directions are determined to be within 90° of the vertical

and 30° of the detector axis are accepted.

During the period November 19, 1972, to March 20, 1973, when the

data to be discussed in this paper were accumulated, over 8000

analyzed gamma rays satisfied these angular criteria and also had

measured energies greater than 35 MeV. Although some gamma rays had

lower measured energies, the effective area solid angle calibration is

less certain at these lower energies; therefore, a lower limit of

35 MeV has been adopted. Almost 12,000 additional analyzed gamma rays

were rejected because they did not not satisfy these criteria, with

the great majority of the rejected gamma rays having zenith angles

greater than 90°--mostly near the earth horizon angle (typically 115°
with respect to the vertical) and, therefore, predominately earth
albedo. For the data on which absolute fluxes were calculated and
reported in this paper, the event selection was normally further
restricted by accepting only gamma rays whose measured arrival direc-
tions were within about 25° of the detector axis because of the in-
creased uncertainty associated with the calibrated sensitivity at wide
angles. Finally, an additional, separate set of earth albedo gamma
rays was analyzed from periods when the telescope was pointed nearly
directly at the earth.

3. Calibration

An extensive program of calibration was conducted for the SAS-2
experiment using both the flight unit and an identical flight spare
unit. In this calibration the efficiency for gamma ray detection was
determined as a function of angle of incidence of the gamma ray and
gamma ray energy over the surface of the telescope. In addition, the
angular resolution was studied as a function of incident energy,
position on the detector, and angle of incidence. Finally, the energy
resolution of the SAS-2 telescope was determined as a function of the
same parameters.

The energy range from approximately 20 MeV to 114 MeV was studied
at the National Bureau of Standards (NBS), Gaithersburg, Maryland, using
the gamma ray beam developed jointly by NBS and GSFC and described by
Hartman et al. (1973). The energy range to 1000 MeV was studied at

DESY, Hamburg, using the tagged gamma ray beam developed for the cali-
bration of the COS-B spark chamber telescope and described by Christ
et al. (1974).

The gamma ray detection capability of the detector can best be
expressed in terms of effective area of gamma ray detection efficiency
as a function of energy and angle with respect to the detector axis
after taking into account the varying efficiency over the telescope
surface in each case. The efficiency is the net efficiency after both
trigger probability and event acceptance criteria, discussed pre-
viously are included. The results are shown in figure 4, which displays
the effective area as a function of energy for four incident angles
with respect to the detector axis.

The angular resolution of the detector has been measured at the
two facilities for the range of energies from 37 MeV to 1000 MeV.
Figure 5 gives the average deviations from the median of the distri-
butions of the reconstituted arrival direction angles as a function
of gamma-ray energy. This parameter is considered more representative
than the frequently used "1σ" value since the distributions differ
significantly from Gaussians. Since the arrival angle is evaluated
independently in the two orthogonal projections the values for the
angular error given in figure 5 are "1-dimensional" and apply directly
when investigating radiation coming from a plane feature like the
galactic disk, but have to be multiplied by a factor of approximately
$\sqrt{2}$ for the full spatial angle error. No significant difference has
been found for the angular resolution when looking at gamma-rays incident

off the detector axis or at an angle with respect to the principal detector axis up to 15° from the vertical. The angular resolution degrades by 25-30% between 15° and 30°. The medians of the recon- stituted arrival direction distributions are found to coincide within uncertainties ($\leqslant \pm 1°$) with the actual beam incidence direction up to the largest angle examined, 30°.

In addition to the calibration at NBS and DESY there were two means of estimating the detection capability of the SAS-2 gamma ray telescope in flight. These are based on the atmospheric albedo and celestial diffuse radiation. The latter made use of the data from high galactic latitudes where the diffuse radiation appears isotropic. This approach gave a post-launch comparison of the angular response of the detector of low statistical weight, but nonetheless one which did confirm the gross features of the calibration. The atmospheric radia- tion measurement agreed within errors with the flux expected from previous measurements (Fichtel et al., 1973a). In the analysis, only gamma rays arriving within an angle of 35° from the nadir were used to avoid large variations with angle.

The final subject related to the calibration work is the energy resolution evaluation and with it the method of converting from a measured spectrum to the primary spectrum. The method used for the individual gamma ray energy evaluation is based on the analysis of the scattering of the two tracks of the electron pair, described in the previous section. Figure 6 shows the distributions of estimated gamma-

ray energies for various incident beam energies, at 0° inclination.
The spread in energy of both the NBS and DESY gamma ray beams is small
compared to the detector energy resolution. It is seen that, although
the energy resolution is limited, a consistent evaluation of the gamma-
energy is possible up to about 200 MeV where the method is no longer
useful because of the predominance of the "reading error" in the
scattering measurement.

In principle, with very good statistics the primary energy
spectrum can be deduced from the measured energy distribution using
a least squares method such as that developed by Trombka and Schmadebeck
(1968). In practice, statistical fluctuations can dominate, leading to
unlikely results or effectively an indeterminate situation from the
standpoint of likely spectra. If, on the other hand, the primary
spectrum is assumed to be smooth over the relatively small energy
range of interest here (about 25 to 500 MeV), then the expected
measured spectrum can be calculated on the basis of the experimentally
measured distribution functions as a function of primary energy. For
the purposes of the work here, it has been assumed that the primary
spectrum was either a power law of the form

$$dJ/dE = KE^{-n} \qquad (1)$$

or a cosmic ray nucleon--nucleon interaction gamma ray spectrum
as calculated for example by Stecker (1970), who uses the measured
cosmic ray energy spectrum and assumes the cosmic rays are incident on
interstellar nuclei essentially at rest. The measured energy distri-
bution that will result for these various primary spectra can then be

calculated and compared to the actually observed spectra. All spectra

discussed in this paper are assumed to be of one of the two forms

mentioned above, or a combination of the two, except for the atmospheric

albedo gamma ray spectrum, for which a spectrum deduced from previous

measurements and theoretical calculations was used (Thompson, 1974).

4. Sensitivity and Intensity Calculations

The reduction of the observed gamma ray intensity to an absolute

celestial intensity or flux requires a knowledge of the relative amount

of exposure to each region of the sky. In addition to an accurate

determination of the detector response this requires a knowledge of

the attitude of the detector axis, the angle of the axis with respect

to the earth vertical vector, the orbital position of the satellite,

the live time of the telescope, the percentage of data lost, and the

status of experiment commands which affect the exposure value. A

program was developed which scans the entire data base for the required

input information and calculates the exposure to any desired region of

the sky, taking into account earth occultation and telescope sensitivity

as a function of detector axis angle. Since the instrument response

varies with gamma ray energy, this calculation must be made as a

function of energy. The sensitivity is computed for 5184 bins of equal

solid angle in the sky. The gamma ray intensity for any bin is then

the ratio of the number of gamma-rays seen for these coordinates to the

product of the sensitivity (including the relative exposure, the

observing time, and the solid angle) and the telescope effective area

for a particular energy range. The relative exposure value is presented in the form of sensitivity contours.

III. EXPERIMENTAL RESULTS AND DISCUSSION

As mentioned in the introduction, the gamma ray observations which have been obtained with SAS-2 divide naturally into four subjects: the strong component from the galactic plane with its hard energy spectrum, the general diffuse radiation, low energy gamma ray bursts, and localized sources. In the discussion that follows, each of these topics will be presented. The experimental results in each case will be accompanied by a discussion of their possible interpretation.

A. Galactic Plane

1. Experimental Results

Relative to the general background celestial diffuse radiation, a strongly enhanced intensity of high energy gamma rays is observed along the entire galactic plane. The energy spectrum of this galactic plane gamma radiation is observed to have a flatter energy spectrum than that of the diffuse celestial radiation to be discussed later in IIIB. The region in ℓ^{II} from about 325° to about 40° is particularly intense, as seen in figure 7, which shows the intensity of gamma rays above 100 MeV summed from $b^{II} = -10°$ to $b^{II} = +10°$ and plotted as a function of galactic longitude in 5° intervals. Notice particularly that the radiation from the galactic center itself is not significantly more intense than the rest of this interval. This lack of a single, strong

peak in the gamma ray distribution at the center excludes the possibility of explaining the general enhancement in the region ($325°$ $< \ell^{II} < 40°$) solely in terms of a theory involving a strong maximum of emission in the galactic center region.

Considering the radiation in the $330°< \ell^{II} < 30°$ interval, figure 8(a) shows the angular distribution in b^{II} for gamma rays with measured energies above 100 MeV. There is clearly a relatively narrow component, which can be shown to be consistent with, or only slightly broader than, the detector resolution alone, discussed in Part IIC. In addition there is a much broader component. The experimental points in figure 8a have been compared to the sum of two curves, one with the detector angular resolution corresponding to a hard spectrum above 100 MeV and the other a gaussian. Two combinations, one 50% a detector resolution function and 50% a gaussian with a 1σ of $6°$, the other 60% a detector resolution function and 40% a gaussian with a 1σ of $7°$, give nearly equally good fits under the χ^2 test. Relatively small variations from these, such as a 40%-60% or a 60%-40% split for the $6°$ gaussian case or any combination with a $5°$ gaussian give a χ^2 at least twice as large. Any attempted fit using a single gaussian produced a χ^2 at least five times as large as the best fit using two curves. In terms of galactic structure, this result implies that the origin of the radiation is about equally divided between close (< 2 or 3 kpcs) and more distant regions, since galactic features beyond about 3 kiloparsecs are narrower in b^{II} than the detector angular resolution.

In figure 8(b) the distribution in b^{II} for gamma rays with measured energies above 100 MeV and with $90° < \ell^{II} < 180°$ and $200° < \ell^{II} < 260°$ is shown. This region excludes the large flux from the Vela and Crab regions. The lack of a narrow peak in this case suggests that most of this radiation is coming from relatively close regions, as expected from the location of the solar system in the galaxy. The other distinctive aspect of figure 8 is the very much greater intensity of the galactic radiation in the $330° < \ell^{II} < 30°$ region, which was also shown in figure 7.

In figure 8, also note that, whereas the 100 MeV gamma radiation approaches the diffuse background level by about $\mid b^{II} \mid = 15°$ on the negative b^{II} side in the center regions, it remains relatively high to $b^{II} = +30°$ on the positive side of the $(330° < \ell^{II} < 30°)$ region. A lesser enhancement is observed on the negative side of the interval $(160° < \ell^{II} < 200°)$. When examined more closely there is a hint that these regions correlate with Gould's Belt, but the limited statistics make it difficult to assign specific locations to the excesses.

A figure similar to figure 7 is obtained when the galactic plane radiation above 100 MeV is plotted in $5°$ ℓ^{II} intervals, but summed only in the interval $(-4° < b^{II} < 4°)$. The principal difference, besides slightly larger uncertainties in individual points, is a larger ratio for the radiation from $(325° < \ell^{II} < 40°)$ to that from $(90° < \ell^{II} < 180°)$ or from $(200° < \ell^{II} < 260°)$, as expected since the narrower, more distant, features are enhanced. The $(75° < \ell^{II} < 80°)$ peak also is somewhat more significant.

Returning to figure 7, the entire excess in the region 260° to 270° lies south of the galactic plane and can be attributed to the region around Vela X, centered about ($\ell^{II} = 3°$, $\ell^{II} = 265°$). The high energy gamma ray excess was reported previously (Thompson et al., 1974) and will be discussed further in Section IIID. The excess in the region ($180° < \ell^{II} < 190°$) can be attributed to the Crab nebula. The remainder of the excess from about 185° to 200° in ℓ^{II} is a few degrees above the galactic plane. The enhanced region starting presumably before $\ell^{II} = 310°$ (there is a gap in data from 290° to 310°) and extending to 50 to 55° corresponds roughly to the angular extent of the strong inner galactic arms. The possible theoretical explanation for the high energy gamma radiation from the galactic plane will be pursued in detail in the next section, IIIA2, along with a more detailed discussion of the relationship of the galactic structure to the gamma radiation.

The energy spectrum of the radiation for the region 330°< ℓ^{II}< 30° is shown in figure 9 after subtracting the diffuse background, which is small--between 6 and 7 percent above 100 MeV. The errors shown result primarily from calibration and energy resolution uncertainties, since over 2400 gamma rays are included in the analysis. After subtracting the diffuse background the energy spectrum from the rest of the galactic plane is similar, or possibly slightly harder. The gamma radiation from the Vela region has an energy spectrum indistinguishable from the rest of the plane.

The average intensity above 100 MeV is seen in figure 9 to be $(0.96 \pm 0.14) \cdot 10^{-4}$ gamma rays/cm^{2}rad sec for the interval $(330° < \ell^{II} < 30°, -10° < b^{II} < 10°)$ after the diffuse background, equivalent to $(0.066 \pm 0.009) \cdot 10^{-4}$ is subtracted. This energy spectrum is consistent with a two component model consisting of a $\pi°$ decay type spectrum and a differential power law of the form $dJ/dE = AE^{-2.0}$, within the limits shown in figure 9.

Other results shown in figure 9 include the results of Kraushaar et al. (1972) and Share et al. (1974a). The high altitude balloon experiments all have the difficult problem of the atmospheric background. Nonetheless, data from these at high energies ($\geq$ 100 MeV), some positive results and other upper limits (Frye et al., 1971; Bennett et al., 1972; Fichtel et al., 1972; Dahlbacka et al., 1973; Sood et al., 1974; Frye et al., 1974), agree with the results shown in figure 9 within rather large uncertainties, except Frye et al. (1974), who report values well below those shown.

2. Discussion

The energetic galactic gamma rays are generally thought to result primarily from the interaction of cosmic rays with interstellar matter. This concept will be examined here in terms of some of the models that have been proposed after a brief review of the parts of the basic calculation of particular importance here.

The number and energy spectrum of the gamma rays produced by cosmic rays interacting with interstellar matter have been calculated

in detail for the case of the cosmic radiation in interstellar
space by several authors, e.g. Stecker (1973) and Cavallo and Gould
(1971) for the proton interactions and Bussard (1974) for the electron
interactions. The flux of gamma rays with energies greater than E
at a distance r is given by the expression

$$\Phi(E) = 1/4\pi \int S(E)g(r,d\theta,d\phi) \, n(r,d\theta,d\phi) \, dr \, (\sin\theta \, d\theta \, d\phi) \quad (2)$$

where S is the number of gamma rays produced per second on the
average for one interstellar nucleon plus electron and a cosmic ray
density and spectrum equal to that near the earth, n is the inter-
stellar number density, and g has been introduced here to represent
the ratio of the cosmic ray density to that in the vicinity of the
solar system. The interstellar nucleon component is primarily of
importance for cosmic ray nuclear particles and the electron for
cosmic ray electrons. However, assuming the galaxy to be neutrally
charged on the average, the net effect of the two phenomena can be
treated together in one equation such as eq. (2).

The principal contribution to the high energy ($\geq 10^2$ MeV) gamma
radiation from the cosmic ray nuclear interactions with interstellar
matter comes in the cosmic ray energy range from a few-tenths of a
GeV to a few tens of GeV. Below that energy range the parent π°
mesons leading to gamma rays are not produced, and at higher energies
the contribution is very small because the cosmic ray energy spectrum
is decreasing much faster with energy ($\sim E^{5/2}$) than the pion produc-
tion is increasing ($\sim E^{1/4}$). The contribution from the cosmic ray

electrons becomes important primarily in the lower part of the gamma ray energy range being considered here. The overall source function $S(E)$ has the value $1.6 \cdot 10^{-25}$/sec above 100 MeV, using for the nucleonic component the value given by Stecker (1973) and for the electrons that given by Bussard (1974), based on the cross sections of Koch and Motz (1959) and the electron spectrum deduced by Goldstein, et. al. (1970).

Compton and synchrotron radiation are generally not thought to be dominant in the production of high energy gamma rays. Compton radiation could originate either from cosmic ray electrons interacting with starlight or the blackbody radiation; however, neither should make a significant contribution unless either the cosmic ray electron density is proportionally much larger elsewhere in the galaxy or starlight should increase dramatically (by almost two orders of magnitude) toward the galactic center. As a consequence, the calculated longitudinal distribution in pure Compton radiation models generally peaks much too sharply at $\ell^{II} = 0°$ (e.g. Coswik, 1974) to be consistent with the observations reported here. Synchrotron radiation will also not be important unless again the field strength increases very rapidly toward the inner part of the galaxy.

In the first attempts to compare the observed high-energy gamma-ray intensity with calculated values, it was assumed (e.g. Kraushaar et al. ,1972) that the cosmic-ray density was uniform throughout the galaxy so that g could be taken outside the integral in eq. (2) and was usually set equal to one. Using the 21-cm data to estimate columnar hydrogen density Kraushaar et al. (1972) showed that whereas

the calculated intensity was fairly close to that expected in the anti-center direction when the expected intensity was integrated over the solid angle of the detector (which had a gaussian angular sensitivity with a 1σ of about 15°), the observed intensity in the galactic center region was about four times the calculated value. Thus, the galactic longitudinal dependence was inconsistent with this model, and it could not be brought into agreement by assuming a uniformly higher value of the cosmic-ray density or by assuming that the total matter density was uniformly much higher because a significant portion of the inter-stellar hydrogen was in molecular form, for example.

More recently, Strong et al. (1973) assumed that the cosmic-ray density has a smooth distribution, but one which increases towards the galactic center in accordance with an expression of Thielheim and Langhoff (1968) representing the mean magnetic field or the square of the mean magnetic field. This work, although not in agreement with present results, was one of the first to break with the constant cosmic-ray density concept.

Stecker et al. (1974) proposed that the galactic cosmic-ray intensity varies with the radial distance from the galactic center and is about an order of magnitude higher than the local value in a toroidal region between 4 and 5 kpc. They further suggest that this enhancement can be plausibly accounted for by Fermi acceleration caused by a hydrodynamic shock driven by the expanding gas in the "4 kpc" arm and invoked in some versions of galactic structure theory. This theory does provide a possible explanation of the general en-

hancement in the central region as shown, but not some of the

other features now beginning to appear. There is, of course, also

the question of whether or not the Fermi acceleration exists. If it

does, then, clearly, the accelerated cosmic-rays could play an

important role.

In pursuing the problem of galactic gamma radiation, it is impor-

tant to realize that the full-width angular resolution of the high-

energy gamma-ray detectors flown thus far has been either several

degrees, in the case of SAS-2, or about 24° in the case of OSO-3.

Thus, the observed intensity of a feature with a thickness comparable

to the disc of the galaxy will decrease approximately as the recip-

rocal of the distance once it is more than 2 kps away from SAS-2

(and closer for OSO-3), and faster if it is also small in extent

within the plane. Hence, more distant regions of the galaxy would

have to be substantially more intense than local ones to explain an

observed intensity of gamma-rays in any given direction with the

present instruments. This consideration, together with the geo-

metrical distribution of the intense high-energy gamma radiation,

particularly the broad distribution of the gamma radiation in galactic

longitude over 70° to 90° in the central region of the galaxy, sug-

gested to Kniffen et al. (1973) that the source of the enhancement is

possibly predominantly diffuse radiation from the spiral arm segments

closest to the sun in the direction of the galactic center.

Bignami and Fichtel (1974) proceeded further and proposed that

in general the cosmic-rays are enhanced where the matter is greatest;

namely, in the arm segments. This hypothesis is supported

by the following considerations: First, it is assumed that the

cosmic-rays and magnetic fields are galactic and not universal. Then,

as shown by Bierman and Davis (1960) and Parker (1966) in more detail,

the magnetic fields and cosmic-rays can only be contained by the weight

of the gas through which the magnetic fields penetrate; and, hence,

they are tied to the matter. The galactic cosmic-ray energy density

cannot substantially exceed that of the magnetic fields, or the

cosmic-ray pressure will push a bulge into the fields ultimately

allowing the cosmic-rays to escape. The local energy density of the

cosmic-rays is about the same as the estimated energy density of the

average magnetic fields and the kinetic motion of matter. Together

the total pressure of these three effects is estimated to be approxi-

mately equal to the maximum that the gravitational attraction can

hold in equilibrium. This suggests that the cosmic-ray density may

generally be as large as would be expected under quasi-equilibrium

conditions. This concept is also given some theoreti-

cal support by the calculated slow diffusion rate of cosmic rays (e.g.

Parker, 1969; Lee, 1972; Wentzel, 1974) in the magnetic fields of the

galaxy based on the cosmic ray lifetime and the small cosmic ray

anisotropy and the likely high production rate of cosmic rays, which

together suggest that in general the cosmic rays should be plentiful

in a given region and will not move quickly to less dense regions.

Therefore, it was assumed that the energy density of the cosmic rays

is larger where the matter density is larger. As a trial assumption,

Bignami and Fichtel (1974) let the cosmic-ray density be proportional to the matter density on the scale of galactic arms. The fluctuations in matter density are then quite important in determining the expected gamma-ray intensity calculated by eq. (2) since the gamma radiation becomes proportional to n^2.

The spatial distribution of interstellar matter has generally been estimated from 21-cm radio data which, however, indicates only atomic hydrogen densities and does not include the ionized and molecular hydrogen. There are in addition some problems associated with the direct interpretation of the 21-cm data as discussed, for example, by Simonson (1970). Relying on measurements from external galaxies and on the density wave theory for the spiral pattern (e.g., Roberts and Yuan, 1970), Bignami and Fichtel (1974) assume that the inner galactic arms had an arm to interarm density ratio of five to one. With this assumption, the center to anticenter ratio and the absolute intensity can be explained as well as the distribution within the 310° $< \ell^{II} < 50°$ interval in the general way permitted by a cylindrical model approximation. With the higher molecular density now thought to exist in the inner part of the galaxy, the arm to inter arm ratio could be reduced substantially and still provide agreement with the experimental results.

In this model, the Sagittarius arm makes a major contribution, and it is close enough in the $\ell^{II} = 0°$ direction that its width in b^{II} is greater than the detector resolution. Figure 8, as noted earlier clearly shows a distribution of at least two components.

Recently Scoville and Solomon (1974b)have used 2.6 mm radio

measurements they have made of the CO emission line to estimate the

molecular hydrogen density distribution in the galaxy based on the

hypothesis (Scoville and Solomon, 1974a;Goldreich and Kwan, 1974)

that the most important source of CO excitation in galactic clouds

is the collision of CO with H_2. Using the cylindrically-symmetric

Schmidt model, they concluded that the molecular hydrogen density is

relatively large, between 1/2 and 5 molecules/cm^3, in the region from

5 to 8 kpcs from the galactic center, with the maximum density between

5 and 6 kpcs. Since this mass density range is from 1 to 10 times

the atomic hydrogen density assumed in most previous work, its contri-

bution to the gamma radiation could be substantial if the higher side

of the range is correct. Cowan et al. (1974) have noted the important

implication of a higher molecular hydrogen density and Solomon and

Stecker (1974) have suggested that this ring could be the major source

of the observed gamma radiation.

Returning to figure 7, the sharp decrease between $\ell^{II} = 50°$ and

55° is consistent with the tangent to the Sagittarius arm as shown in

figure 10 (Simonson, 1973). The valley from 50° to 70° is consistent

with the lack of features in that direction and the increase in Cygnus

from 70° to 80° is consistent with the direction of the Orion arm.

In addition to the central arms making a strong general con-

tribution, actual peaks in the gamma radiations are expected at

directions along the galactic arms. Maxima would then be expected

between 310° and 315°, 330° and 335°, and 340° and 345° in ℓ^{II} cor-

responding to the Scutum, Norma and 4 kpc arms. Peaks in these regions are indeed seen in figure 7. Whereas any one peak may not be considered statistically significant (The error bars in figure 7 included more than the statistical uncertainty), the fact that all three peaks are observed is clearly a striking feature. On the other side of the plane the arms are closer to the sun and not as clearly separated; however, the 4 kpc and Scutum arm tangents fall in the 20° to 40° interval and only Sagittarius of the strong inner arms is left beyond 40°, consistent with the observations. There also appears to be a contribution from the galactic center itself, or other sources in that direction.

These results suggest that all the principal galactic arm segments between the solar system and the galactic center are playing a significant role in the origin of the high energy gamma radiation, and, although the 4 kps "ring" may be making an important contribution, it is not necessarily dominating the gamma radiation observed at the earth. The combination of the galactic longitudinal and latitudinal distributions seem to support well the concept of cosmic rays and matter being concentrated into arm segments, although the determination of the molecular hydrogen is most important to a complete understanding of this situation.

Point or localized sources of gamma rays may be making a contribution to the galactic intensity in addition to those already mentioned. It will most probably not be possible to determine if they are a significant contribution until gamma ray telescopes with

better angular accuracy than SAS-2 are flown. It has been suggested that the steep spectra of most of the X-ray sources speak against many significant gamma ray point sources in the galaxy, but, since gamma ray production mechanisms are very different, the gamma ray sky probably looks very different from the X-ray sky, just as the X-ray sky looks very different from the optical sky. Hence, the question must remain open.

At present, the high energy galactic gamma radiations seems adequately explained as resulting primarily from cosmic ray inter- actions with matter, and this explanation is supported not only by the magnitude of the radiation, but its galactic longitudinal and latitudinal distribution.

B. Diffuse Radiation

1. Experimental Results

One of the areas of interest for the SAS-2 experiment is the study of a possible diffuse component of the celestial gamma ray intensity, especially since such a diffuse intensity would probably originate outside the galaxy. Measurements of this radiation could, therefore, provide information and constraints on theories involving extragalactic cosmic ray and matter densities, both at the present and in the cosmo- logical past, and on antimatter distributions such as those proposed in the baryon symmetric big bang cosmology.

The OSO-3 gamma ray experiment of Kraushaar, et. al,(1972) observed an apparently diffuse intensity for regions of the sky which did not

include the galactic plane. An integral value of $(3.0 \pm 0.9) \cdot 10^{-5}$ photons/$(cm^2 sec\ sr)$ was obtained for the intensity above 100 MeV, but essentially no energy spectral information was available. In a previous paper, preliminary results from SAS-2 showed that the diffuse intensity had a steep energy spectrum (Fichtel, et. al., 1973b)

SAS-2 data from six regions of the sky away from the galactic plane have now been examined. A uniform, apparently diffuse, intensity has been measured for that portion of these regions with $| b^{II}| > 30°$. The detector pointing directions were ($\ell^{II} = 0°$, $b^{II} = +25°$), ($\ell^{II} = 0°$, $b^{II} = +58°$), ($\ell^{II} = 19°$, $b^{II} = -23°$), ($\ell^{II} = 190°$, $b^{II} = -30°$), ($\ell^{II} = 285°$, $b^{II} = +75°$), and ($\ell^{II} = 300°$, $b^{II} = -45°$). Only gamma rays arriving within 25° of the detector pointing direction were accepted for analysis.

The data with $| b^{II}| > 30°$ from these regions show a gamma ray intensity which is uniform in both intensity and energy spectrum, within statistics. Data from these areas have been combined into the diffuse energy spectrum shown in figure 11. This differential energy spectrum is steeper than any other spectra observed on SAS-2 or the earlier balloon work of this group with a similar detector (e.g. Fichtel, et. al., 1969, and Fichtel, et. al, 1972). The shaded area represents the diffuse spectrum seen by SAS-2, unfolded from the detector response, along with the uncertainty in the measurement. Representing the energy spectrum by a power law of the form $dJ/dE = AE^{-\alpha}$ photons/$(cm^2\ sec\ sr\ MeV)$ over the SAS-2 energy range of 35 to 200 MeV, α is found to be 2.4 ± 0.2. The integral flux above 100 MeV is measured to be $(1.93 \pm 0.26) \cdot 10^{-5}$

photons/(cm^2 sr sec), wherein the error includes statistical, calibration, and energy resolution uncertainties, but not any effect resulting from possible region to region variations.

The only non-celestial background contribution to this gamma ray component is that due to interactions of cosmic ray particles within the material surrounding the detector, principally the 0.15 g/cm^2 thick thermal blanket. Such interactions would have to produce a gamma ray in the field of view of the detector without leaving a charged particle with energy and direction such as to trigger the anticoincidence system. Monte Carlo calculations indicate that this contribution is well over an order of magnitude below the measured diffuse intensity even at the highest energies considered by SAS-2. Additional evidence against a significant background for this component is the observed spectral distribution which is totally different from the spectrum expected from cosmic ray interactions in the detector material.

The integral flux value reported here lies somewhat below the OSO-3 result (Kraushaar, et. al., 1972), but the two values agree within errors, and the OSO-3 result probably contains a small local galactic component since considerable data with $|b^{II}| < 30^\circ$ (and even some with $|b^{II}| < 15^\circ$) were included as a result of the rather wide acceptance angle of the OSO-3 detector (FWHM $\approx 24^\circ$). The SAS-2 results are seen to be in agreement with the upper limits set by other experiments (Bratolyubova, et. al, 1971; Hopper, et. al, 1973; Share, et. al, 1974b) but disagree with the observation of Herterich, et. al, (1973).

Taken as a whole, the measurements of the diffuse gamma ray spectrum do not present a simple picture. The line labeled B in figure 11 is

a plot of the function $dJ/dE = 0.011 \; E^{-2.3}$ in units of photons/ $(cm^2 sec \; sr \; MeV)$ with E expressed in MeV. This line was chosen to pass through both the SAS-2 data and the < 1 MeV gamma ray data. This curve is also consistent with the high energy x-ray data within uncertainties (Schwartz and Gursky, 1973; Dennis, et. al., 1973). However, the majority of the data from 1 to 10 MeV seem to lie above and have a flatter spectral shape than this power law would indicate, implying first a decrease and then an increase in spectral slope. The intensity in the 5 to 40 MeV energy range is quite uncertain at this time.

2. Discussion

Until more regions of the sky are included in the SAS-2 data, no statement is possible concerning the degree of uniformity of the radiation away from the galactic plane. The steep spectrum observed by SAS-2 away from the galactic plane lends weight to the hypothesis that this radiation is not simply a combination of many sources with the type of gamma ray source mechanism seen in our own galaxy.

Under the assumption that the regions of the sky already examined are representative of a diffuse celestial intensity, the theoretical implications can be considered. Whenever cosmic rays and matter coexist, gamma rays are produced by nuclear collisions, and, once produced, gamma rays in the energy range viewed by SAS-2 suffer very little attenuation in space. These facts make possible the use of the SAS-2 observations to set limits on the extent of the region in which cosmic rays can exist at a level comparable to that observed at earth. Several assumptions must be made in order to set such limits, the first of which

is the choice between an open and closed universe. Under the assumption

of a closed universe, a reasonable estimate for the intergalactic

matter density is about 10^{-5} protons/cm^3. With this matter density,

cosmic rays could not exist at the local level beyond a radius of about

50 Mpc, since the resultant gamma ray intensity above 150 MeV as

calculated from equation (2) would then be higher than what has been

observed by SAS-2. Thus, a cosmic ray density equal to that near the

earth cannot pervade a closed universe, but the possibility that cosmic

rays at the local density exist throughout our local supercluster of

galaxies cannot be eliminated. The open universe permits much lower

intergalactic densities, but it is then necessary to consider specific

cosmological models because contributions from large distances and

hence high redshifts are involved. These considerations will be treated

shortly, together with other possible origins for the diffuse radiation.

The list of candidate models to explain the diffuse radiation is

lengthy, and an analysis of many of these would be beyond the scope of

this paper. Nevertheless, from the point of view of the SAS-2 measure-

ments, several of these models deserve attention. The basic features

of the diffuse gamma ray spectrum which any model must explain are the

apparent spectral flattening in the 1 to 10 MeV energy range and the flux

and steep spectrum above 30 MeV.

The diffuse gamma rays may originate from diffuse electrons

interacting with matter, photons, or magnetic fields. Bremsstrahlung

seems unlikely, since, in an energy region, 1 to 10 MeV, where an

increased slope would be expected due to an increasing rate of energy loss,

the opposite is observed. For both synchrotron and Compton radiation, the observed photon spectrum would imply a similarly-shaped parent electron spectrum which would have even sharper spectral features. Further, for all three cases, the observed intensity seems high to be consistent with reasonable estimates of the interstellar parameters.

Of the pure gamma-ray cosmological hypotheses, there are at least three that seem to be possible candidates. They are particle-antiparticle annihilation in the baryon symmetric big bang model, the cosmic-ray-intergalactic matter interaction model, and the cosmic-ray-blackbody interaction model. In all theories, the resulting gamma-ray spectrum is red-shifted substantially by the expansion of the universe.

Harrison (1967) was one of the first to propose a model of the big bang theory of cosmology with the principle of baryon-symmetry. Omnes (1969), following Gamow (1948), considered a big-bang model in which the universe is initially at a very high temperature and density, and then showed that, if the universe is baryon-symmetric, a separation of matter and antimatter occurs at $T > 30$ MeV. The initial phase separation of matter and antimatter leads ultimately to regions of pure matter and pure antimatter of the size of galaxy clusters. Stecker, Morgan, and Bredekamp (1971) have predicted the gamma ray spectrum which would be expected from π^o decay arising from the annihilation of nucleons and antinucleons at the boundaries of such clusters from the beginning of their existance to the present. This spectrum is shown in figure 11.

In an expanding model of the universe, the density of matter is much greater in the cosmological past than in the present, and if cosmic

rays are present they interact with this matter leading to gamma rays whose energies are once again red-shifted as observed at the present time. One curve developed by Stecker (1969) involving red-shifts up to about 100 is essentially indistinguishable from curve A in figure 11 in the energy range for which data exists and is not shown for this reason. This model does imply, however, an implausibly high cosmic ray energy density at early times in the universe.

A third cosmological model involves cosmic ray interactions with the blackbody radiation at an early point in cosmological time. Wolfendale (1974) has shown that this theory is also a possibility.

For the present the origin and nature of the diffuse gamma ray intensity must remain an open question. In particular, both the large- and small-scale uniformity of the diffuse radiation need to be established more firmly, together with improved determination of the energy spectrum at all energies.

C. Low Energy Gamma Ray Bursts

In 1973, Klebesadel et al. (1973) reported the detection of low energy gamma ray bursts, and they have subsequently been confirmed by other groups. The most recent catalog of these bursts is that of Strong et al. (1974). Although the high energy gamma ray telescope of SAS-2 in itself has a threshold of about 20 MeV, the SAS-2 anticoincidence dome provides a very large detector for the high energy portion ($\gtrsim 0.3$ MeV) of these events. From any side or the top of the SAS-2 experiment, there is an effective area of about $2.5 \cdot 10^3 \text{cm}^2$. The energy threshold varies with position over the 1.5cm thick dome and with incident

angle at any one point. However, except in the vicinity of the bottom

rim its response is fairly uniform. Averaging over the dome it is

found that the effective threshold for detection is about 0.15 MeV,

the average efficiency rising to about 20% at 0.6 MeV. The counting

rate of the anticoincidence dome when there is no increase due to the

trapped radiation in the Atlantic anomaly* is about $4.2 \cdot 10^3$ cts/sec.

and it remains quite steady.

During the period of its operation, November 20, 1972, through

June 8, 1973, SAS-2 detected two events observed by other satellites

and discovered one, which was later confirmed by other satellites. In

addition, two events on the list of those detected by Vela were not seen

by SAS-2. In view of the high sensitivity of SAS-2, these negative

results suggest that the earth occulted the source, as it will 40%

of the time on the average. Table 1 gives a list of these five events.

With regard to the two events not seen by SAS-2, if it is assumed

that the absence of a detectable signal in the SAS-2 A-dome is an earth

occulation effect rather than a large energy spectral effect, then a

region of the sky in which the event had to occur can be established.

These are a 70° cone about $\alpha = 36.6°$, $\delta = 1.0°$ in the case of the

18 December 1972 event and a similar cone about $\alpha = 27.4°$, $\delta = 1.6°$

in the case of the 7 May 1973 event. For the Dec. 18, 1972 event, this

cone is consistent with the location of the source lying   in the

* The earth's trapped radiation extends downward to unusually low
altitudes in the central and south Atlantic. These low energy electrons
and protons cause an increase in the A-dome count rate. It has little
other effect on the gamma ray telescope since the A-rate is not high
enough to cause a significant dead time and the high energy trapped
particle rate is not sufficient to produce false coincidences.

TABLE 1

DATE	TIME	SATELLITE
18 December, 1972	20:27:39	2 Velas$_1$[1]; IMP-7[3]; 1972-076B[4]
2 March , 1973	23:27:53	2 Velas$_1$[1]; IMP-7[3]; SAS-2[5]
7 May , 1973	08:04:32	3 Velas$_2$[2]
6 June , 1973	07:07:28	IMP-7[3]; SAS-2[5]
6 June , 1973	18:47:08	SAS-2[5]; IMP-7[3]; 2 Velas[1]

List of low energy gamma ray bursts during the period November 20, 1972 to June 8, 1973. The satellite listed first is the one from which data first led to the event's recognition.

1. Klebesadel, et al., 1974
2. Strong, et al., 1974
3. Cline and Desai, 1974
4. Imhof et al., 1974
5. This paper

region $70° < \alpha < 120°$, $0° < \delta < 20°$ as determined by Imhof et al. (1974) except, of course, it excludes the highest part of the α range. The time history of the 2 March 1973 event as measured by SAS-2 is shown in figure 12. Notice that the time given by the Vela satellites for the first detection of an increase is well into the event. This feature is one indication of the considerably greater sensitivity of the SAS-2 A-dome, although it must be kept in mind that the Vela system triggers on a sudden increase, whereas the SAS-2 search was made on the basis of a threshold effect. The complex structure of this event, which has four distinct peaks, is evident even with limited time resolution. The event reaches a peak intensity of $9.4.10^4$ cts/sec., over two orders of magnitude greater than the threshold of 7×10^2 cts/sec. which the event must surpass in the .768 second readout interval in order to be selected in the computer scan of the SAS-2 data. From earth occultation consid-erations of SAS-2, the event had to occur in a region of the sky within

a cone of 110° of ($\alpha = 49.4°$, $\delta = 0.1°$). Vela data (Klebesadel et al., 1974) indicates the source had to be in a circular band of radius $82.5 \pm 4°$ centered at $\alpha = 173.9°$, $\delta = 25.7°$.

It is interesting that the other two events seen by SAS-2 occurred on the same day, 6 June, 1974. The time profiles of these two events are shown in figure 13. The second of these two events was found in the SAS-2 data before it had been noted elsewhere. There were, in fact, only three detected cases in the approximately 6 1/2 months that the A-dome rate exceeded the threshold level and remained above background (by $> 3 \cdot 10^2$ cts/sec) for more than three readout intervals (approximately 2.3 seconds), except when the satellite passed through the Atlantic trapped radiation anomaly. Hence, the second June 6 event immediately attracted interest as a possible burst event, and it was subsequently confirmed by the IMP-7 satellite (Cline and Desai, 1974) and the Vela system (Klebesadel, et. al., 1974). Notice that again for the June 6 event which did trigger the Vela system the Vela time for first detection occurs after the event has started and reached a level almost an order of magnitude above the SAS-2 threshold. In view of the significantly greater sensitivity of SAS-2 as suggested by these comparisons and direct calculations, it is especially surprising that no other events of more than two seconds were observed beyond the three mentioned. From SAS-2 earth occultation considerations the two June 6, 1973, events would have had to occur within 110° of $\alpha = 184.1°$, $\delta = 1.2°$ in the case of the first event and $\alpha = 317.7°$, $\delta = -1.9°$ for the second event.

There was no reported solar activity during any of these events. In

none of the three events were there any high energy gamma rays in the spark chamber. This is not a surprising result because with the given solid angle of the high energy telescope there is less than a 10 percent chance that any of three events would fall within the high energy gamma ray telescope acceptance angle even if there were a detectable flux of > 20 MeV gamma rays in these hard x-ray - low energy gamma ray bursts.

D. Localized Sources

Gamma ray astronomy has been limited in its search for localized sources by the lack of good angular resolution, low counting statistics, and the atmospheric background in the case of balloon experiments. The SAS-2 experiment provides a sensitivity for the detection of discrete sources over an order of magnitude better than that of previous measurements. The marked improvement results from the combined factors of increased sensitivity, better angular resolution, and reduced background. Substantial improvements are still possible over the SAS-2 experiment for future gamma ray telescopes.

Positive fluxes have already been reported from SAS-2 for the Crab nebula (Kniffen, et. al., 1974) and the Vela region (Thompson, et. al., 1974). The Crab emission, observed during the period December 14 to 21, 1972, is characterized by a strong pulsed component from NP0532 with both the pulsed and unpulsed components consistent with a power law extension of observations at lower energies extending to at least a GeV. The total flux above 100 MeV is observed to be $(3.2 \pm 0.9) \cdot 10^{-6}$ photons/cm^2 sec). The Vela emission above 100 MeV is observed to be $(5.0 \pm 1.2) \cdot 10^{-6}$ photons/cm^2 sec) and above 35 MeV is $(1.1 \pm 0.3) \cdot 10^{-5}$ photons/cm^2 sec). Thompson, et. al. (1974) have pointed out the possible

association of this excess emission with the Vela supernova remnant with the implication that approximately $3 \cdot 10^{50}$ ergs of cosmic rays from the supernova are contained in the remnant, although the possibility that a portion of the excess is due to galactic arm segments cannot be eliminated.

A comparison has been made of gamma ray arrival times from the Vela region with predicted pulse arrival times for PSR 0833-45. Pulsar data at 2388 MHz (period, period derivative, and phase) were supplied by Reichley (1974) for the week during which the SAS-2 observations were made (February 15-20, 1973); the arrival times were corrected by 50.3 msec for dispersion. The gamma ray data were plotted as a function of pulse phase, using the same program previously applied to the Crab nebula data. No enhancement was seen in phase with the radio pulse and the upper limit for pulsed gamma rays above 35 MeV in phase with the radio data is $2.1 \cdot 10^{-6}/(cm^2$ sec). This upper limit corresponds to a value of $1.1 \cdot 10^{-6}$ MeV$/(cm^2$ sec MeV), averaged from 35 to 100 MeV, which seems inconsistent with a power law extension to higher energies of the recently reported positive pulsed flux at 10-30 MeV of $1.5 \cdot 10^{-5}$ MeV$/(cm^2$ sec MeV) (Albats, et. al., 1974). The gamma ray data do show a small peak, following the radio pulse by 11 msec. The probability of such a peak appearing by chance in one of the 33 bins used is about 6 percent, and a positive result is not claimed here. Based on this peak, the upper limit for a pulsed gamma ray flux above 35 MeV from PSR 0833-45, at the radio period, would be $5.1 \cdot 10^{-6}/(cm^2$ sec).

In addition to these two established high energy gamma ray sources, the SAS-2 data show other enhancements and provide upper limits on other possible sources. As mentioned in section IIIA., two general regions with $15° < |b^{II}| < 30°$ along the galactic plane show excesses. The SAS-2 detector also saw an apparent excess of high energy radiation a few degrees above the galactic plane from about $\ell^{II} = 185°$ to $\ell^{II} = 200°$, which is too broad to be consistent with a single point source. One object of interest in that region is IC443 ($\ell^{II} = 189°$, $b^{II} = +3°$), a rather old (~60,000 y) supernova remnant, the distance of which has been evaluated to be about 1.5 kpc. The shell of this object shows optical and radio evidence of interactions with the adjacent HII region Sh 249 ($\ell^{II} = 191°$, $b^{II} = +4°$) and a system of HI clouds, the density of which has been estimated to be about 10 to 20 atoms/cm^3 (Akabane, 1966; Duin et al., 1973). Recent observations have shown that IC 443 is an X-ray emitter (Winkler and Clark, 1974).

In the Cygnus region, the enhanced interval from 70 to 80 degrees in galactic longitude has already been mentioned in section IIIA to coincide with the long line-of-sight path length along the Orion arm. It is worth noting, on the other hand, that the Ilovaisky and Lequeux (1972) catalog of supernova remnants list nine such objects with $0° < b^{II} < 6°$ and $74° < \ell^{II} < 83°$, of which two have distance estimates less than 2 kpc. An additional remnant in this general region is the Cygnus Loop, which is south of the plane.

Table 2 presents significant new upper limits on objects of interest for which no evidence of a positive gamma ray flux is obtained with SAS-2.

A 95 percent confidence upper limit of $9.5 \cdot 10^{-7}/(cm^2 \, sec)$ is obtained

for > 100 MeV gamma ray emission from Sco X-1, the most intense x-ray

source. An upper limit of $1.5 \cdot 10^{-6}/(cm^2 \, sec)$ is obtained for the dark

clouds near ρ Oph and in Corona Austrina, suggested by Black and Fazio

(1973) as possible origins for the gamma ray excesses reported for the

directions $\ell^{II} \approx 352°$, $b^{II} \approx 16°$ (Dahlbacka, et. al., 1973) and $\ell^{II} \approx 0°$,

$b^{II} \approx -19°$ (Frye, et. al., 1969; Frye, et. al., 1971). The upper

limits obtained with SAS-2 fall over an order of magnitude below the

reported fluxes but do not conflict with the theoretical prediction.

Limits (> 100 MeV) for other previously reported gamma ray sources

within the analyzed regions include $1.2 \cdot 10^{-6}/(cm^2 \, sec)$ for the

region $\ell^{II} = 340.7°$, $b^{II} = 30.3°$ (Frye, et. al., 1971), and $2.0 \cdot 10^{-6}/$

$(cm^2 \, sec)$ for $\ell^{II} = 163.8°$, $b^{II} = -9.5°$ (Frye, 1972). These again

lie at least an order of magnitude below the quoted fluxes. A limit

of $2.5 \cdot 10^{-6}/(cm^2 \, sec)$ is obtained for 3C120, over two orders of

magnitude below the flux observed by Volobuev, et. al., (1971) from

this general direction.

Table 2

SAS-2 Localized Source Limits (>100 MeV)

(95 Percent Confidence)

Object	Periods of Observation (see note below)	ℓ^{II} (Degrees)	b^{II} (Degrees)	Flux limit (10^{-6} photons/cm^{2}sec)
Galaxies				
Large Magellanic Cloud	12	280	-33	2.4
Small Magellanic Cloud	12	303	-45	1.0
M31	17	121	-21	1.4
M87	9	283.6	+74.5	1.0
Supernova Remnants				
Lupus Loop	1	330.1	+15.1	2.4
Monoceros Nebula	8	205.5	+0.2	4.4
Cas A	16,17	111.7	-2.1	1.1
Cygnus Loop	15	74.0	-8.6	1.4
HB 21	16	89.1	+4.7	1.2
CTA 1	17	119.5	+10.0	1.1
Tycho's SNR(3C10)	17	120.4	+1.4	1.1
X-Ray Sources				
Sco X-1 (3U1617-15)	7	359.1	+23.8	0.95
Cyg X-1 (3U1956+31)	15	71.3	+3.1	2.7
Cyg X-2 (3U2142+38)	16	87.3	-11.3	1.2
GX5-1 (3U1758-25)	2,10	5.0	-1.0	2.9
GX1+4 (3U1728-24)	2,10	1.4	+3.9	4.0
GX3+1 (3U1744-26)	2,10	3.0	+1.0	2.8
Other Objects				
ρ Oph	2,7,10	353	+17	1.5
Corona Austrina	2,10	360	-18	1.5
Jupiter	11	19.8	-22.1	0.63

Periods of Observation

1	11/20/72	to	11/27/72
2	11/28/72	to	12/5/72
7	1/4/73	to	1/11/73
8	1/11/73	to	1/17/73
9	1/17/73	to	1/23/73
10	1/24/73	to	1/31/73
12	2/8/73	to	2/14/73
15	3/1/73	to	3/6/73
16	3/6/73	to	3/13/73
17	3/13/73	to	3/19/73

IV. SUMMARY

The results from the Second Small Astronomy Satellite gamma ray
experiment reported here have revealed a number of aspects of high
energy gamma ray astronomy;

1. The galactic gamma radiation, which dominates over the
    diffuse radiation along the entire galactic plane, is
    most pronounced in a region from $\ell^{II} = 335°$ to $\ell^{II} = 40°$.

2. When examined in detail the longitudinal and latitudinal
    distribution seem generally correlated with galactic
    structural features, and particularly with arm segments.

3. On the basis primarily of its angular distribution and magnitude,
    the general high energy gamma radiation from the galactic
    plane seems to be explained best as resulting primarily from
    cosmic ray interactions with interstellar matter.

4. High energy gamma ray astronomy then holds the promise of
    being able to map the high energy cosmic ray gas in the galaxy
    and study the disturbing effects of the cosmic ray pressure.
    Further, since the penetrating power of gamma rays is so high,
    an unclouded view of the galaxy should ultimately be possible.

5. From the study of six different regions of the sky with
    $\mid b^{II} \mid > 30°$, there appears to be a uniform celestial gamma
    radiation, as suggested by earlier results, especially Kraushaar
    et al. (1972). Over the energy range from about 35 MeV to
    170 MeV, the differential energy spectrum has the form

$$\frac{dJ}{dE} = (2.7 \pm 0.5)(\frac{E}{100})^{-2.4 \pm 0.2} \frac{\text{gamma rays}}{\text{cm}^2 \text{ sr sec MeV}}$$

where E is expressed in MeV.

6. The interpretation of the diffuse flux depends critically on the determination of the flux in the 0.6 to 35 MeV regions. If the apparent flattening of the spectrum in the 0.6 to 10 MeV region is verified, the high energy results presented here, when combined with the lower energy data, suggest a cosmological origin for this radiation.

7. Three low energy gamma ray bursts were observed in the large SAS-2 anticoincidence scintillator in the period from November 19, 1972 to June 8, 1973. The two seen in coincidence with the Vela satellites began at earlier times than those given by Vela. Considerable structure was seen in two of the three events. In view of the high sensitivity of the anticoincidence scintillator, it is perhaps significant that more events were not seen, especially that no smaller events were observed.

8. In addition to the general galactic emission, high energy gamma radiation was seen from the Crab nebula (a significant fraction of which is pulsed at the radio pulsar frequency), Vela-X (a supernova remnant whose high energy gamma radiation possibly provides the first direct experimental evidence associating cosmic rays with supernovae), the general region $(15° < b^{II} < 30°, 340° < \ell^{II} < 20°)$, and a region a few degrees

north of the galactic plane around 190° to 195° in ℓ^{II}.

9. Several upper limits to high energy gamma ray fluxes were also set, including $1.0 \cdot 10^{-6}$ for the Small Magellanic Cloud, $9.5 \cdot 10^{-7}$ for Sco X-1, $2.5 \cdot 10^{-6}$ for 3C120, $1.0 \cdot 10^{-6}$ for M-87, and $1.1 \cdot 10^{-6}$ for CasA, in units of photons (E>100 MeV)/cm^2 sec.

- 50 -

APPENDIX

The formalism for the application of multiple scattering measurements to the determination of electron energies in a multiplate spark chamber has been given by Pinkau (1966, 1968) and Kniffen (1969). From this work it can be easily shown that for a probability distribution $f(x,\phi,y)$ for an electron at depth x in the chamber (Fig. A1), the probability distribution for obtaining successive displacements y, y' and y" at depths x, x+mΔ and x+nΔ in a spark chamber with gap separation Δ (Fig. A2) is given by

$$W(y,y',y'') = \iiint d\phi d\phi' d\phi'' \Delta f(m\Delta,\phi-\phi',y-y'-m\Delta\phi') \times f(n\Delta,\phi'-\phi'',y'-y''-n\Delta\phi'').$$

(A1)

Representing $f(x,\phi,y)$ by its Fourier transform

$$f(x,\phi,y) = \frac{1}{(2\pi)^2} \iint_{-\infty}^{\infty} d\eta_1 d\eta_2 F(x,\eta_1,\eta_2) e^{i\phi\eta_1+iy\eta_2}$$

W becomes

$$W(y,y',y'') = \frac{1}{(2\pi)^4} \iiint d\phi d\phi' d\phi'' \iint d\eta_1 d\eta_2$$

$$\times F(m\Delta,\eta_1,\eta_2) e^{i\eta_1(\phi-\phi')+i\eta_2(y-y'-m\Delta\phi')}$$

$$\times \iint d\eta_3 d\eta_4 F(n\Delta,\eta_3,\eta_4) e^{i\eta_3(\phi'-\phi'')+i\eta_4(y'-y''-n\Delta\phi'')}$$

(A2)

Using the relationship $\int_{-\infty}^{\infty} e^{i\eta\phi} d\phi = 2\pi\delta(\eta)$, $W(y,y',y'')$ becomes

$$W(y,y',y'') = \frac{1}{2\pi nm\Delta} \int_{-\infty}^{\infty} d\eta F(m\Delta,o,\frac{\eta}{m\Delta}) F(n\Delta,\eta,\frac{-\eta}{m\Delta})$$

$$\times e^{\frac{i\eta}{\Delta}(\frac{my-(n+m)y'-ny''}{nm})}$$

(A3)

From moliere scattering theory (Moliere, 1955), it can be shown (Pinkau, 1966) that the dominant term of the Fourier transform function is given by

$$F(n\Delta, \eta_1, \eta_2) = \exp[-J_d^2(u_n\eta_1^2 + v_n\eta_1\eta_2 + w_n\eta_2^2)]$$

with

$$u_n = nd$$
$$v_n = n^2 d\Delta$$
$$w_n = n\frac{d}{4}(\Delta^2 + \frac{d^2}{3}) + \frac{(n+1)n(n-1)}{3} d\Delta^2$$

where

$$J_d = \frac{1}{X_o} \frac{112}{\log 183\ Z^{-1/3}} \frac{z^2}{(pv)^2} B_d, \quad \frac{1}{B_d} e^{B_d} = \frac{6.68\times10^3}{\beta^2} \frac{d}{A} \frac{(Z+1)Z^{1/3}z^2}{(1+3.34\alpha^2)} \quad ,$$

$d = d_o/\cos\langle\phi\rangle$, where $\langle\phi\rangle$ is the average angle of the particle trajectory through the scattering plate, d_o is the plate thickness, X_o is the radiation length of the scattering material with atomic number Z and mass A, $\alpha = \frac{zZ}{137\beta}$, and z and β are the charge and velocity of the electron. Hence

$$F(m\Delta, 0, \frac{\eta}{m\Delta}) = \exp[-\frac{J_d^2}{4} (w_m \frac{\eta^2}{m^2\Delta^2})]$$

and

$$F(n\Delta, \eta, \frac{-\eta}{n\Delta}) = \exp[-\frac{J_d^2}{4}(u_n\eta^2 - v_n\frac{\eta^2}{n\Delta} + w_n\frac{\eta^2}{n^2\Delta^2})].$$

Defining $\beta_{mn} = ny - (n+m)y' + my''$, W then becomes

$$W(\beta_{mn}) = \frac{1}{2\pi} \iint_{-\infty}^{\infty} d\eta\ F(m\Delta, 0, n\eta)F(n\Delta, mn\Delta\eta, -mn)e^{i\eta\beta_{mn}}$$

$$= \frac{1}{2\pi} \int_{-\infty}^{\infty} d\eta\ \exp[-\frac{J_d^2}{4}\eta^2][w_{mn}^2 + u_n n^2 m^2\Delta^2 - v_n m^2 n\Delta + w_n n^2]e^{i\eta\beta_{mn}}.$$

(A4)

Defining

$$Q_{mn}^2 = [w_n n^2 + u_n n^2 m^2 \Delta^2 - v_n m^2 n \Delta + w_n m^2] = w_m n^2 + w_n m^2 ,$$

$$W(\beta_{mn}) = \frac{1}{2\pi} \int_{-\infty}^{\infty} d\eta \ \exp[- \frac{J_d^2 \eta^2}{4} Q_{mn}^2] e^{i\eta\beta_{mn}} = \frac{2}{J_d Q_{mn} \sqrt{\pi}} \exp[\frac{\beta^2}{J_d^2 Q_{mn}^2}] ;$$

(A5)

and hence

$$<|\beta|>_{mn} = \frac{J_d Q_{mn}}{\sqrt{\pi}} .$$

It follows by definition that

$$<pv> = \frac{K_d Q_{mn}}{<|\beta|>_{mn}}$$

(A6)

where $K_d = (pv)\frac{J_d}{\sqrt{\pi}}.$

Using this result, it is possible to make use of all spark data points where spark chamber inefficiencies might otherwise prevent it.

In practice, the situation is complicated by the presence of reading noise which introduces an uncertainty δy in the measured spark position. Defining

$$n_{mn} = [2(m^2 + mn + n^2)]^{1/2} \delta y ,$$

the measured $<|\beta|>_{mn}$ becomes

$$<|\beta|>_{mn} = [(K_d Q_{mn})^2 + n_{mn}^2]^{1/2} .$$

The weighted summation of the combined readings of different combinations of all lengths must be done with careful consideration of the statistics and the significance of the scattering signal. The method chosen for SAS-2 analysis is given by

$$\frac{1}{(pv)} = [\Sigma \eta_{mn} \omega_{mn}]^{-1} \Sigma \frac{\eta_{mn} \omega_{mn}}{K_d Q_{mn}} [<|\beta|>_{mn}^2 - n_{mn}^2]^{1/2} \qquad (A7)$$

where η_{mn} is the number of readings of type mn and ω_{mn} is a weighting factor defined by

$$\omega_{mn} = [\frac{K_d Q_{mn}}{(pr)_c} - n_{mn}]$$

$(pr)_c$ is taken to be the characteristic energy for the particular spark chamber configuration and is chosen to be 80 MeV for SAS-2.

The reading noise is a function of the angle of the track, with respect to the chamber axis. To correct for this effect, n_{mn} in Equation (A7) has been replaced by $n_{mn}(1 + a<\phi>_i + b<\phi>_i^2)$ where "a" and "b" were determined experimentally and $<\phi>_i$ is the average projected angle with respect to the vertical in the x or y view, as specified by the subscript i. It was found in the calibration data that a small residual angular correction was necessary for the highest energy gamma rays, since no set of "a" or "b" values satisfied the entire energy range; this correction was applied as a direct multiplying factor at high energies.

REFERENCES

Agrinier, B., Forichon, M., Leray, J.P., Parlier, B., Montmerle,
    T., Boella, G., Maraschi, L., Sacco, B., Scarsi, L., DaCosta,
    J.M., and Palmeira, R. 1973, Proceedings of 13th Internation-
    al Cosmic Ray Conference,1, 8.

Akabane, R. 1966, Publ. Astron. Soc. Japan, 18, 96.

Albats, P., Frye, G.M., Jr., Thomson, G.B., Hopper, V.D., Mace, O.B.,
    Thomas, J.A. and Staib, J.A. 1974, "Pulsed 10-30 MeV γ-rays
    from PSR 0833-45," preprint, submitted to Nature.

Bennett, K., Penengo, P., Rochester, G.K., Sanderson, T.R. and
    Sood, R.K. 1972, Nature, 238, 31.

Bierman, L. and Davis, L. 1960, Zs. f. Ap., 51, 19.

Bignami, G.F. and Fichtel, C.E. 1974, Ap. J. Letters, 189, L65.

Black, J.M. and Fazio, G.G. 1973, Ap. J. Letters, 185, L7

Bratolyubova-Tsulukidze, L.I., Grigorov, N.L., Kalinkin, L.F., Melio-
    ransky, A.S., Pryakhin, E.A., Savenho, I.A., Yufarkin, V. Ya 1971,
    Geomagnetism and Aeronomy (Soviet), 11, 585.

Bussard, R. 1974, private communication.

Cavallo, G. and Gould, R.J. 1971, Nuovo Cim.,2B, 77.

Christ, H., Peters, F., Bignami, G.F., Burger, J.J., Hermsen, W.,
    Paul, J.A., Pfeffermann, E., Taylor, B.G., Voges, W.H. and
    Willis, R.D. 1974, Nuc. Inst. and Methods, 116, 477.

Cline, T. and Desai, U. 1974, private communication (to be published).

Cowan, J.J, Kafatos, M. and Rose, W.K. 1974, "Sources of Excitation
    in the Interstellar Gas and Galactic Structure," U. of Mary-
    land preprint.

Cowsik, R. 1974, "Geometry of Inverse Compton Gamma Ray Sources," COSPAR
    Proceedings, IIIA.1.4.

Dahlbacka, G.H., Freier, P.S. and Waddington, C.J. 1973, Ap. J., 180,
    371.

Daniel, R.R., Joseph, G. and Lavakare, P.J. 1972, Ap. and Space Sci.,
    18, 462.

Dennis, B.R., Suri, A.N. and Frost, K.J. 1973, Ap. J., 186, 97.

Derdeyn, S.M., Ehrmann, C.H., Fichtel, C.E., Kniffen, D.A. and Ross,
    R.W. 1972, Nuc. Inst. and Methods, 98, 557.

Duin, R.M., Strom, R.G. and Van der Laan, H. 1973, in Supernovae and
    Supernova Remnants (Ed. C.B. Cosmovici), D. Reidel, Dortrecht, Holland, 295.

Fichtel, C.E., Kniffen, D.A. and Ögelmann, H.B. 1969, Ap. J., 158, 193.

Fichtel, C.E., Hartman, R.C., Kniffen, D.A. and Sommer, M. 1972,
    Ap. J., 171, 31.

Fichtel, C.E., Hartman, R.C. and Kniffen, D.A. 1973a, Proceedings of
    13th International Cosmic Ray Conference, 1, 302.

Fichtel, C.E., Hartman, R.C. and Kniffen, D.A. 1973b, Ap. J. Letters,
    186, L99.

Frye, G.M., Jr. 1972, summarized by G.G. Fazio in X- and Gamma-Ray Astronomy
    (Ed. H. Bradt and R. Giacconi), D. Reidel, Dortrecht, Holland, 303.

Frye, G.M. Jr., Albats, P.A., Zych, A.D., Staib, J.A., Hopper, V.D.,
    Rawlinson, W.R. and Thomas, J.A. 1971, Nature, 231, 372.

Frye, G.M., Jr., Albats, P., Thomson, G.B., Hopper, V.D., Mace, O.B.
    and Thomas, J.A. 1974, ESLAB Symposium on Gamma Ray Astronomy
    Frascati (Italy).

Galper, A.M., Kirillov-Gyryumov, V.G., Luchkov, B.I., Ozerov, Yu. V.
    1973, Proceedings of 13th International Cosmic Ray Conference,

$\underline{1}$, 450.

Gamow, G. 1948, Phys. Rev., $\underline{74}$, 505.

Goldreich, P., and Kwan, J. 1974, to be published in <u>Ap. J.</u>

Goldstein, M.L., Ramaty, R. and Fisk, L.A. 1970, Phys. Rev. Letters
$\underline{24}$, 1193.

Golenetskii, S.V., Mazets, E.P., Il'inskii, V.N., Aptekar', R.L.,
Bredov, M.M., Gur'yan, Yu. A., and Panov, V.N. 1971, Ap.
Letters, $\underline{9}$, 69.

Harrison, E.R. 1967, Phys. Rev. Letters, $\underline{18}$, 1011.

Hartman, R.C., Fichtel, C.E., Kniffen, D.A., Thompson, D.J., Ögelman,
H.B. and Tümer, T. 1973, Proceedings of 13th International Cos-
mic Ray Conference, $\underline{4}$, 2733.

Herterich, W., Pinkau, K., Rothermel, H. and Sommer, M. 1973, Pro-
ceedings of 13th International Cosmic Ray Conference, $\underline{1}$, 21.

Hopper, V.D., Mace, O.B., Thomas, J.A., Albats, P., Frye, G.M., Jr.,
Thomson, G.B. and Staib, J.A. 1973, Ap. J. Letters, $\underline{186}$, L55.

Hutchinson, G.W., Pearce, A.J., Ramsden, D., and Wills, R.D. 1971,
Proceedings of 11th International Cosmic Ray Conference, $\underline{1}$, 87.

Ilovaisky, S.A. and Lequeux, J. 1972, Astron. and Ap., $\underline{18}$, 169.

Imhof, W.L., Nakano, G.H., Johnson, R.G., Kilner, J.R., Reagan, J.B.,
Klebesadel, R.W. and Strong, I.B. 1974. "Spectral Measurements
of a Cosmic Gamma Ray Burst with Fast Time Resolution," to be
published in <u>Ap. J.</u>

Klebesadel, R.W., Strong, I.B. and Olsen, R.A. 1973, Ap. J. Letters,
$\underline{182}$, L85.

Klebesadel, R.W., Olsen, R.A. and Strong, I.B. 1974, private commu-
nication.

Kniffen, D.A. 1969, NASA Tech. Report TR R-308.

Kniffen, D.A., Hartman, R.C., Thompson, D.J. and Fichtel, C.E. 1973, Ap. J. Letters, 186, L105.

Kniffen, D.A., Hartman, R.C., Thompson, D.J., Bignami, G.F., Fichtel, C.E., Ögelman, H. and Tümer, T. 1974, "Gamma Radiation from the Crab Nebula above 35 MeV," NASA/GSFC preprint, submitted to Nature.

Koch, M.W. and Motz, J.W. 1959, Rev. Mod. Phys., 31, 920.

Kraushaar, W.L., Clark, G.W., Garmire, G.P., Borken, R., Higbie, P., Leong, V. and Thorsos, T. 1972, Ap. J., 177, 341.

Kuo, Fu-Shong, Frye, G.M., Jr., and Zych, A.D. 1973, Ap. J. Letters, 186, L51.

Lee, M.A. 1972, Ap. J., 178, 837.

Mazets, E.P., Golenetskii, S.V., Il'inskii, V.N., Gur'yan, Yu. A. and Kharitonova, T.V. 1974, "Diffuse Cosmic Gamma-radiation Background in the 28 KeV - 4.1 MeV Range from Cosmos 461 Observations," A.F. Joffe Physico Technical Inst. preprint No. 468.

Moliere, G. 1955, Zeit. für Naturforschung, 10a, 177.

Omnes, R. 1969, Phys. Rev. Letters, 23, 38.

Parker, E.N. 1966, Ap. J., 145, 811.

Parker. E.N. 1969, Space Sci. Rev., 9, 654.

Pinkau, K. 1966, Zeit. für Physik, 96, 163.

Pinkau, K. 1968, "Investigation of Spark Chamber Systems with Respect to Power of Resolution in Energy, Position and Direction," Max-Planck-Institut für Physik und Astrophysik preprint.

Reichley, P. 1974, private communication.

Roberts, W.W. and Yuan, C. 1970, Ap. J., 161, 887.

Schönfelder, V. and Lichti, G. 1974, Ap. J. Letters, 191, L1.

Schwartz, D. and Gursky, H. 1973, in Gamma Ray Astrophysics (ed. F.W.

    Stecker and J.I. Trombka), U.S. Govt. Printing Off., Wash., 15.

Scoville, N.Z. and Solomon, P.M. 1974a, Ap. J. Letters, 187, L67.

Scoville, N.Z. and Solomon, P.M. 1974b, to be published in Ap. J.

Share, G.H., Kinzer, R.L. and Seeman, N. 1974a, Ap. J., 187, 45.

Share, G.H., Kinzer, R.L. and Seeman, N. 1974b, Ap. J., 187, 511.

Simonson, S.C., III, 1970, Astron. & Astrophys., 9, 163.

Simonson, S.C., III, 1973, "Density-Wave Map of the Galactic Spiral

    Structure," Univ. of Md. preprint.

Solomon, P.M. and Stecker, F.W. 1974, "Radio and Gamma Ray Evidence

    for a Molecular Arm Feature at 5 kpc from the Galactic Center,"

    ESLAB Symposium on Gamma Ray Astronomy, Frascati (Italy).

Sood, R.K., Bennett, K., Clayton, P.G. and Rochester, G.N. 1974,

    ESLAB Symposium on Gamma Ray Astronomy, Frascati (Italy).

Stecker, F.W. 1969, Ap. J., 157, 507.

Stecker, F.W. 1970, Ap. and Space Sci., 6, 377.

Stecker, F.W. 1973, Ap. J., 185, 499.

Stecker, F.W., Morgan, D.L. and Bredekamp, J. 1971, Phys. Rev.

    Letters, 27, 1469.

Stecker, F.W., Puget, J.L., Strong, A.W. and Bredekamp, J.H. 1974,

    Ap. J. Letters, 188, L59.

Strong, I.B., Klebesadel, R.W. and Olsen, R.A. 1974, Ap. J. Letters,

    188, L1.

Strong, A.W., Wdowczyk, J. and Wolfendale, A.W. 1973, in Gamma Ray Astrophysic_

    (ed. F.W. Stecker & J.I. Trombka), U.S. Govt. Printing Off., Wash., 239.

Thielheim, K.O. and Langhoff, W. 1968, J. Phys. A. (Proc. Phys. Soc.)

    Ser. 2, 1, 694.

Thompson, D.J. 1974, J. Geophys. Res., $\underline{79}$, 1309.

Thompson, D.J., Bignami, G.F., Fichtel, C.E. and Kniffen, D.A. 1974, Ap. J. Letters, $\underline{190}$, L51.

Townsend, M.R. 1969, NASA Technical Note TND-5099.

Trombka, J.I. 1974, private communication.

Trombka, J.I., Metzger, A.E., Arnold, J.R., Matteson, J.L., Ready, R.C., and Peterson, L.E. 1973, Ap. J., $\underline{181}$, 737.

Trombka, J.I. and Schmadebeck, R.L. 1968, NASA SP-3044.

Valentine, D., Kaplon, M.F. and Badhwar, G. 1971, Proceedings of 11th International Cosmic Ray Conference, $\underline{1}$, 101.

Vedrenne, G., Albernhe, F., Martin, I. and Talon, R. 1971, Astr. and Ap., $\underline{15}$, 50.

Volobuyev, S.A., Galper, A.M., Iyudin, A.F., Kirillov-Ugryumov, V.G., Luchkov, B.I. and Ozerov, Yu. V. 1971, Proceedings of 12th International Cosmic Ray Conference.

Wentzel, D.G. 1974, Annual Review of Astronomy and Astrophysics, $\underline{12}$, to be published.

Winkler, P.F. and Clark, G.W. 1974, Ap. J. Letters, $\underline{191}$, L67.

Wolfendale, A.W. 1974, Royal Society Discussion Meeting (Feb.).

FIGURE CAPTIONS

Fig. 1   -- Schematic diagram of the SAS-2 Gamma-Ray Experiment

(Derdeyn, et. al, 1972).

Fig. 2   -- Readout display of a gamma ray pair production event in the

spark chamber shown in two orthogonal views. The X's and Y's

denote cores set due to the passage of charged particles

in the x and y view, respectively. The vertical axis has

been compressed by a factor of 2.7 relative to the horizontal

axis.

Fig. 3   -- Regions of the sky viewed by SAS-2, using a circle drawn

about the viewing axis with a radius corresponding to the

angle at which the sensitivity for detection of gamma rays

is .4 to .5 the value along the detector axis, depending

on energy. The blackened regions are those used for the

results of this paper.

Fig. 4   -- SAS-2 effective area for gamma ray detection, as a function

of gamma ray energy, based on calibrations at the National

Bureau of Standards (points N) and the Deutsches Elektronen-

Synchrotron (points D). The points represent the fractional

detection efficiency times the detector area, averaged

over the surface of the detector, including all acceptance

criteria for gamma rays as described in the text. The

angles shown are between the beam direction and the detector

axis. The solid lines are fits to the experimental data

points. Also shown for comparison are sample points from a

detailed Monte Carlo calculation of the detector efficiency (points X), which agrees with the calibration data.

Fig. 5 -- Angular resolution for the SAS-2 detector, based on calibrations at NBS (points N) and DESY (points D). The values represent the average deviation from the median of the measured gamma ray arrival directions, evaluated separately in the two orthogonal views. The solid line is a fit to the data.

Fig. 6 -- Energy measurement and resolution of the SAS-2 detector, based on calibrations at NBS and DESY. For the beam energies shown, the histograms show the percentage of gamma ray events with energies measured in each of seven energy bins. The energy measurement uses the multiple scattering technique discussed in the text.

Fig. 7 -- Distribution of high-energy (>100 MeV) gamma rays along the galactic plane. The SAS-2 data are summed from $b^{II} = -10°$ to $b^{II} = +10°$. The diffuse background level is shown by a dashed line. The error bars reflect calibration, energy resolution, and statistical uncertainties.

Fig. 8 (a) -- Distribution of high-energy (>100 MeV) gamma rays summed from $\ell^{II} = 330°$ to $\ell^{II} = 30°$ as a function of b^{II}. The diffuse background is indicated by a dashed line.

(b) -- Distribution of high energy (>100 MeV) gamma rays summed from $90° < \ell^{II} < 170°$ and $200° < \ell^{II} < 260°$, where data exists, as a function of b^{II}. The diffuse background is indicated by a dashed line.

Fig. 9   -- Energy spectrum for gamma rays from the region ($-10° < b^{II}$

$< +10°$, $330° < \ell^{II} < 30°$). The shaded region shows the

spectrum measured by SAS-2, unfolded from the detector

response, together with its uncertainty. Data shown for

comparison is from Kraushaar, et. al (1972), shown by an

open circle, and Share, et. al. (1974a), shown by a solid

point. Other results and upper limits are discussed in the

text.

Fig. 10   -- A smoothed spatial diagram of the locations of the maxima

of the matter density deduced from 21-cm HI line measurements

and the density wave theory (Simonson, 1973).

Fig. 11   -- Diffuse celestial radiation observed by several experiments.

The shaded area represents the SAS-2 data unfolded from the

detector response, together with its uncertainty. Other

results are:

         Bratolyubova-Tsulkidze, et. al. (1971)

         Golenetskii, et. al. (1971)

         O   Vedrenne, et. al. (1971)

         Δ   Daniel, et. al. (1972)

         Kraushaar, et. al. (1972) (Assuming $E^{-2.4}$ spectru

         \   Trombka, et. al. (1973) and Trombka (1974)

         □   Kuo, et. al. (1973)

         Hopper, et. al. (1973)

         ◇   Agrinier, et. al. (1973)

         ●   Herterich, et. al. (1973)

$\uparrow$ Share, et. al. (1974b)

$\vdash\!\!+\!\!\dashv$ Mazets, et. al. (1974)

$\blacktriangledown$ Schonfelder and Lichti (1974)

The line B is the function $0.011\ E^{-2.3}$ photons/(cm^2 sec

ster MeV), as discussed in the text. The dashed lines A

and T represent the calculations of Stecker, et. al. (1971)

based on the matter-antimatter annihilation of the baryon-

symmetric cosmology (A) and the annihilation curve plus a

low energy power law component (T). The curves have been

normalized to reflect recent measurements. The results

of Vedrenne, et. al. (1971) and Daniel, et. al. (1972) are

shown without error bars. The estimated uncertainty in

these points is 50%.

Fig. 12   -- Time history of the low energy gamma ray burst observed in

the SAS-2 anticoincidence dome on March 2, 1973. The arrow

shows the event time observed by the Vela satellites

(Klebesadel, et. al., 1974). The counting rates shown are

the excess counts above the steady SAS-2 background of

$4.2 \cdot 10^3$ cts/sec.

Fig. 13   -- Time histories of two gamma ray burst events seen by the

SAS-2 anticoincidence dome on June 6, 1973. The arrows

show the event times observed by the Vela satellites

(Klebesadel, et. al., 1974). The counting rates shown are

the excess counts above the steady SAS-2 background of

$4.2 \cdot 10^3$ cts/sec.

PINCH FRAME

UPPER SPARK CHAMBER

GUARD SCINTILLATION COUNTER

SCINTILLATOR

LOWER SPARK CHAMBER

LIGHT PIPES (4)

PRESSURE VESSEL

CERENKOV COUNTER ASSEMBLY (4 UNITS)

PHOTO-MULTIPLIERS (8)

ELECTRONICS BOXES (4)

PHOTOMULTIPLIERS (4)

MOUNTING CLIPS (8)

PEDESTAL

DUST COVER
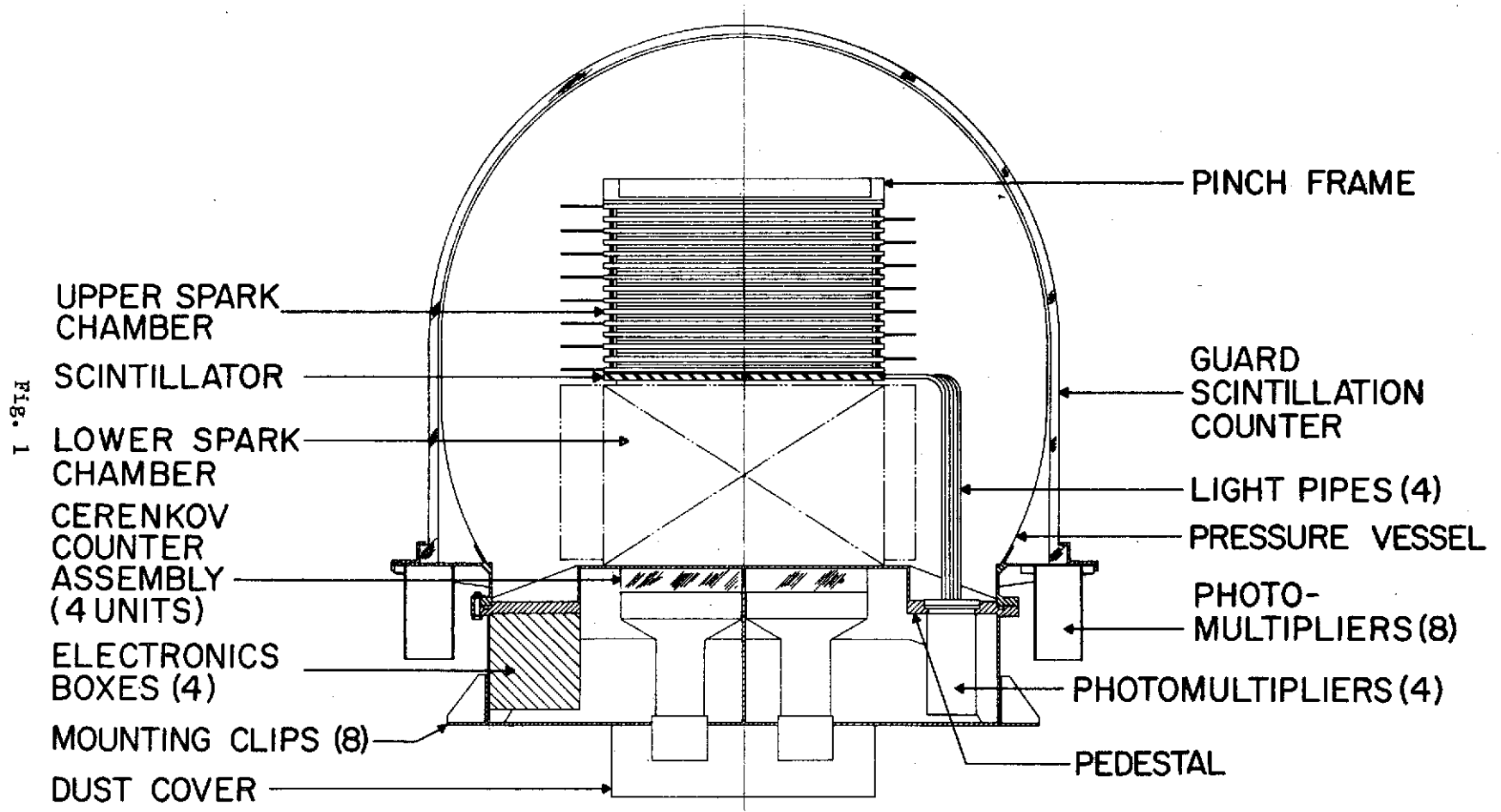
SAS-B GAMMA RAY EXPERIMENT

Fig. 1

Fig. 2

X·ARRAY

Y·ARRAY

EVENT

****

YEAR

72

MO

12

DAY

21

HR

22

MIN

40

SEC

9

MSEC

520

Fig. 3

GAMMA RAY ENERGY (MeV)

Fig. 4

Fig. 5

GAMMA RAY ENERGY (MeV)

SAS-2 ANGULAR RESOLUTION

BEAM ENERGY

1000 MeV

500 MeV

200 MeV

120 MeV

85 MeV

50 MeV

37 MeV

27 MeV

PERCENTAGE

MEASURED GAMMA RAY ENERGIES

Fig. 6

FIG. 7

γ-RAYS (>100 MeV)/(CM^2 RAD SEC)

$(-10° < b^{II} < 10°)$

1×10^{-4}

$.5 \times 10^{-4}$

150° 180° 210° 240° 270° 300° 330° 0° 30° 60° 90° 120° 150°

ℓ^{II}

Fig. 8

PHOTONS (E ≥ 100 MeV)/(CM² SEC STER)

6.0×10^{-4}
5.0×10^{-4}
4.0×10^{-4}
3.0×10^{-4}
2.0×10^{-4}
1.0×10^{-4}

(a)
CENTER

(b)
ANTICENTER
(EXCLUDING CRAB REGION)

BKGD.

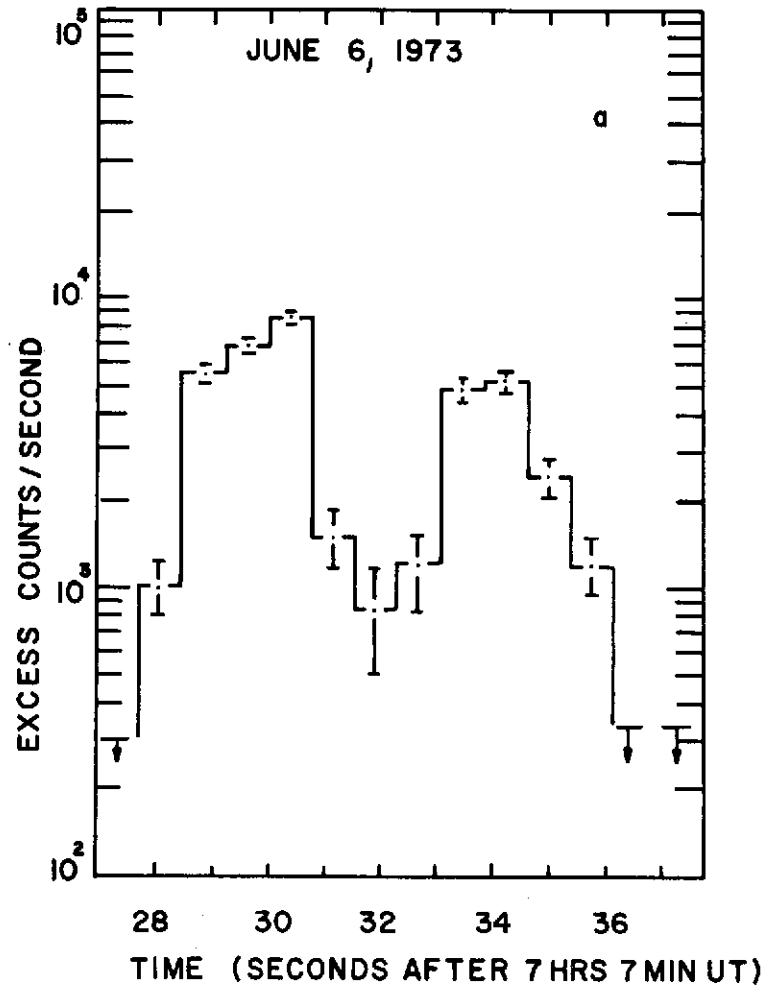-40   -20   0   20   40

-20   0   20

b^{II}

b^{II}
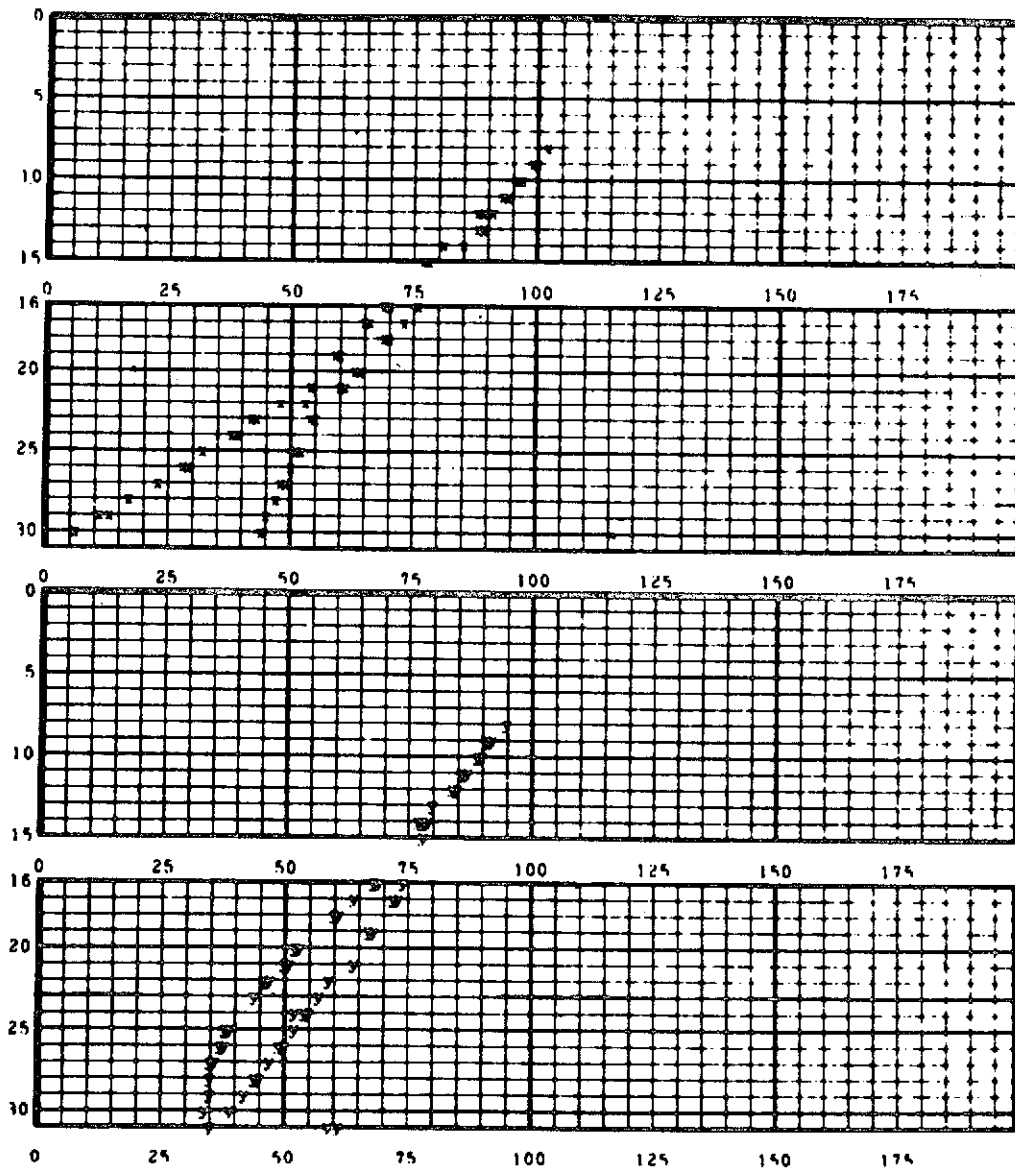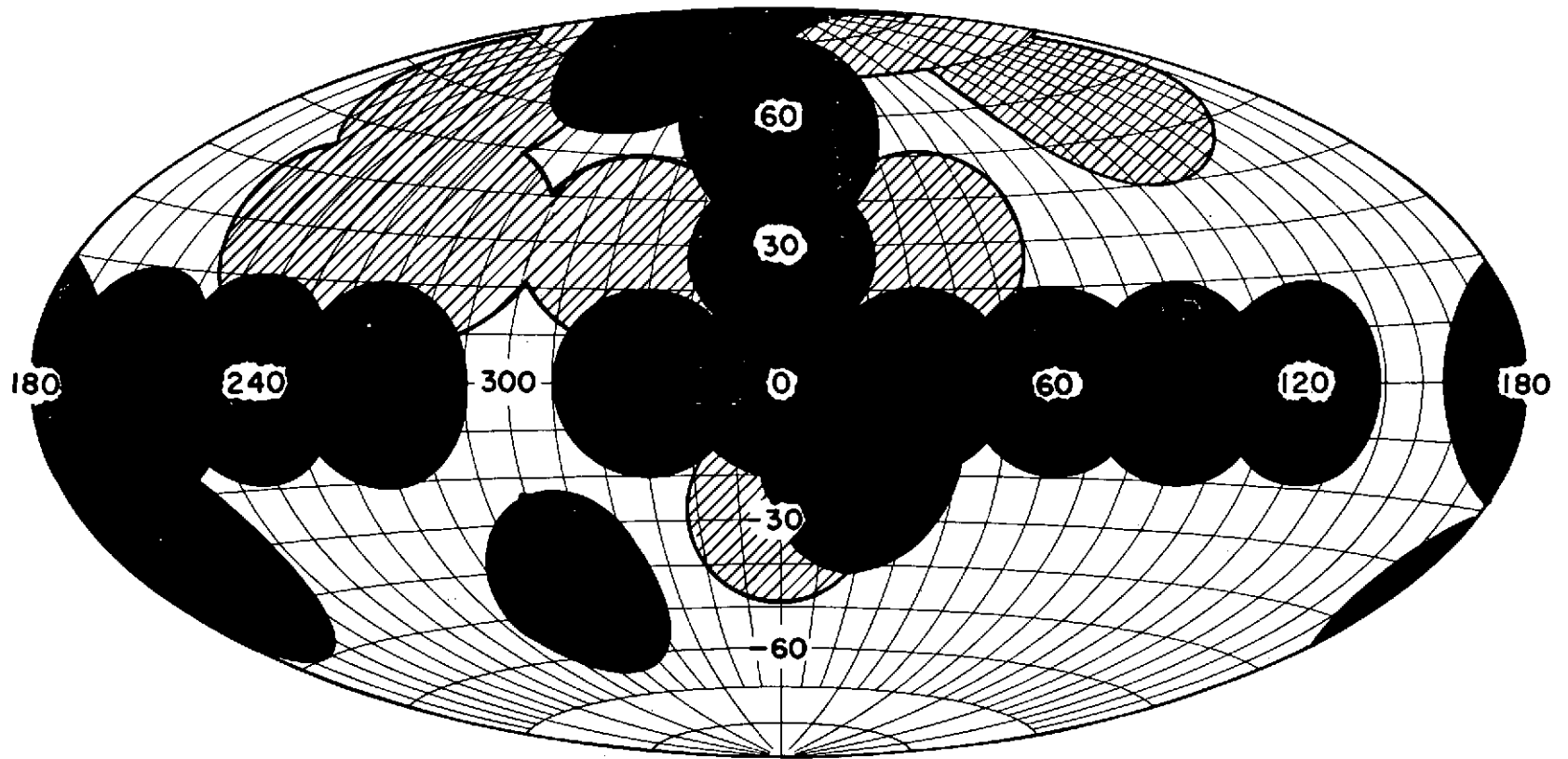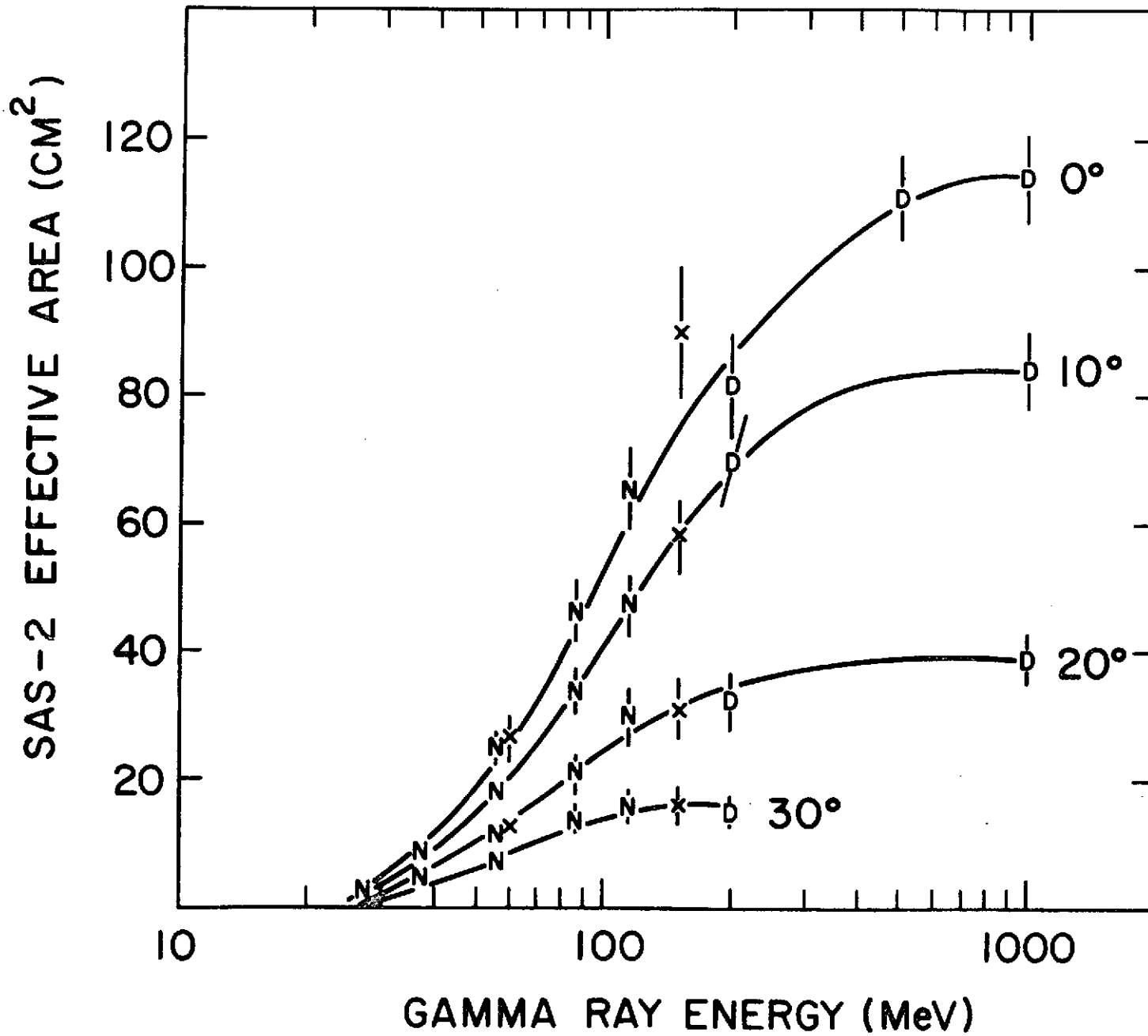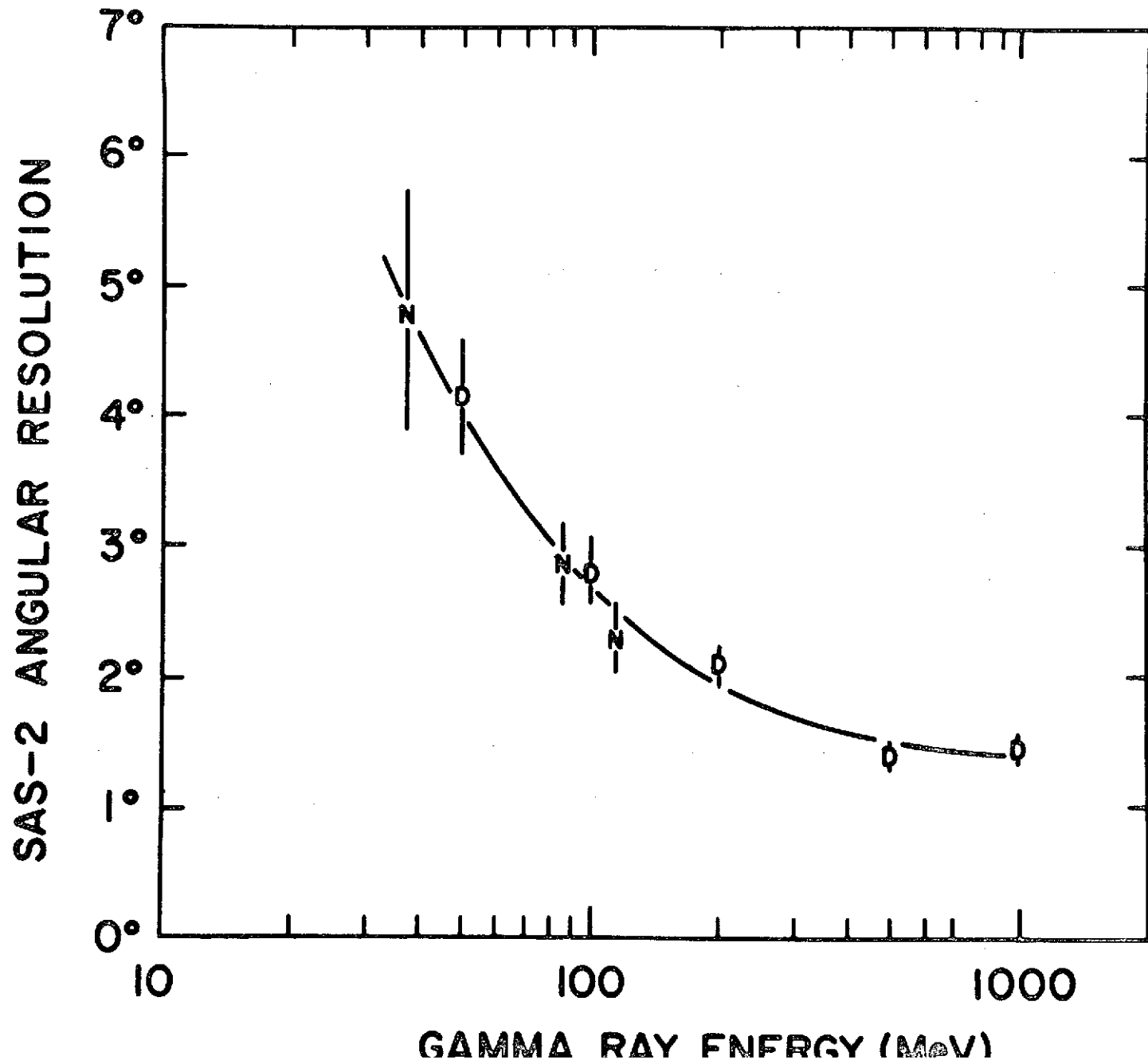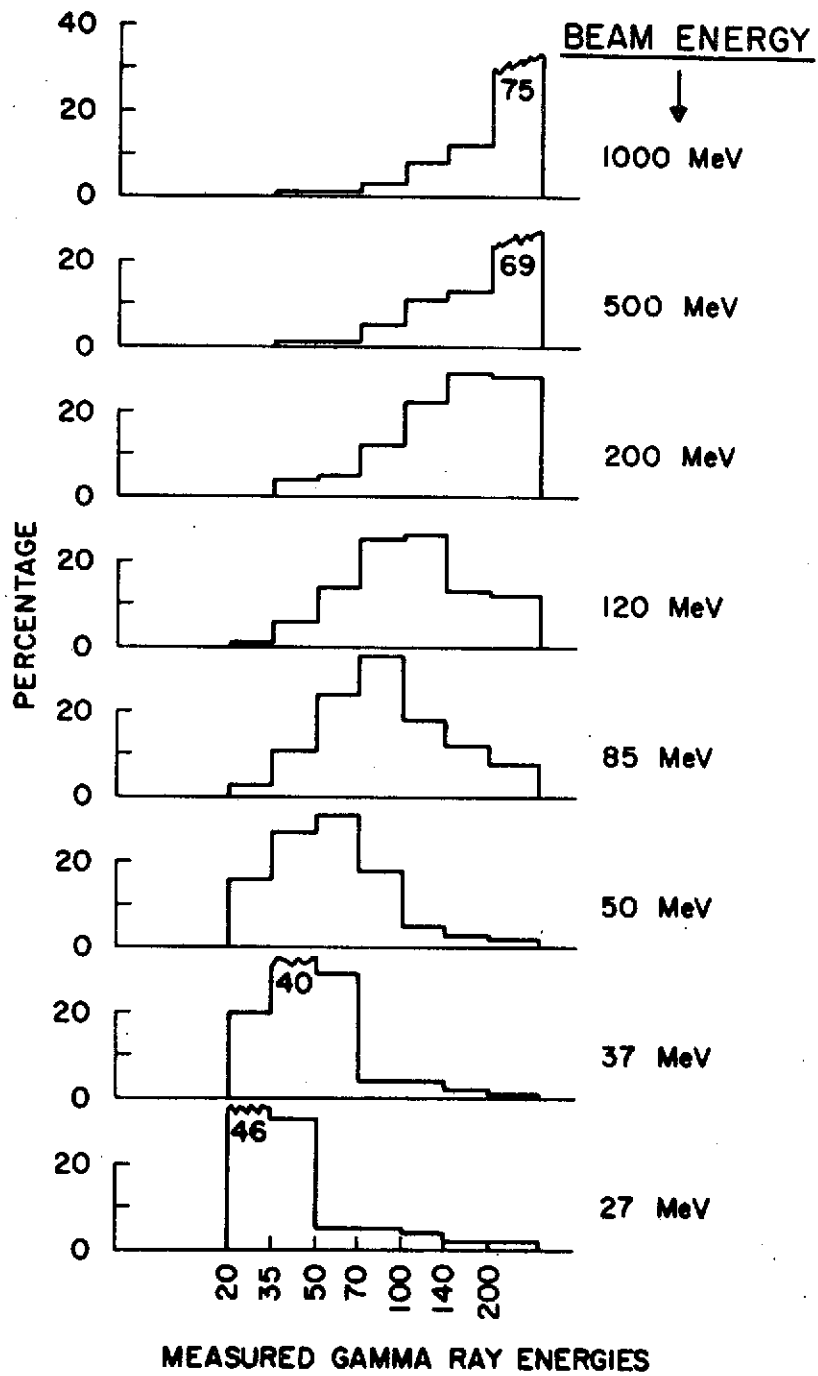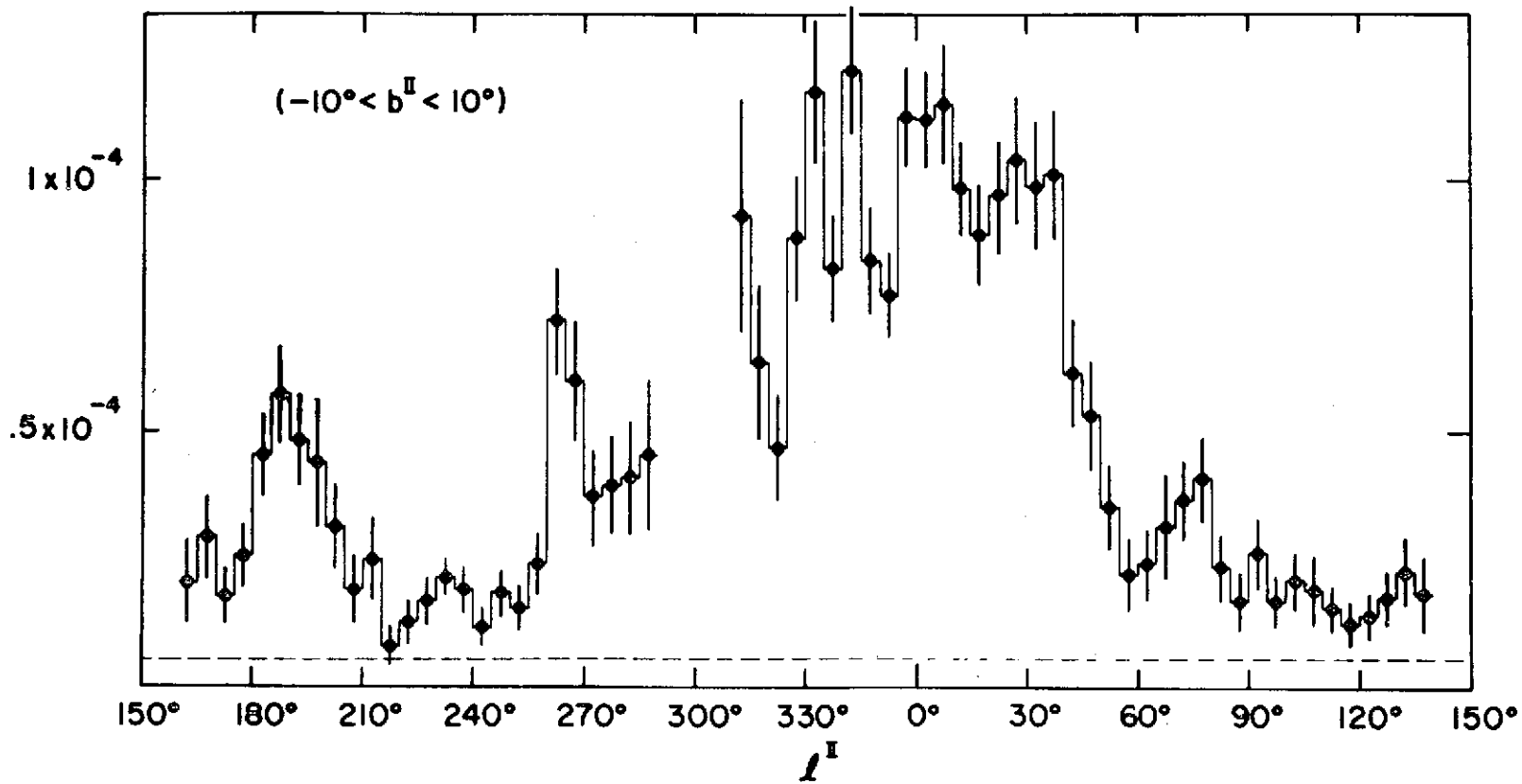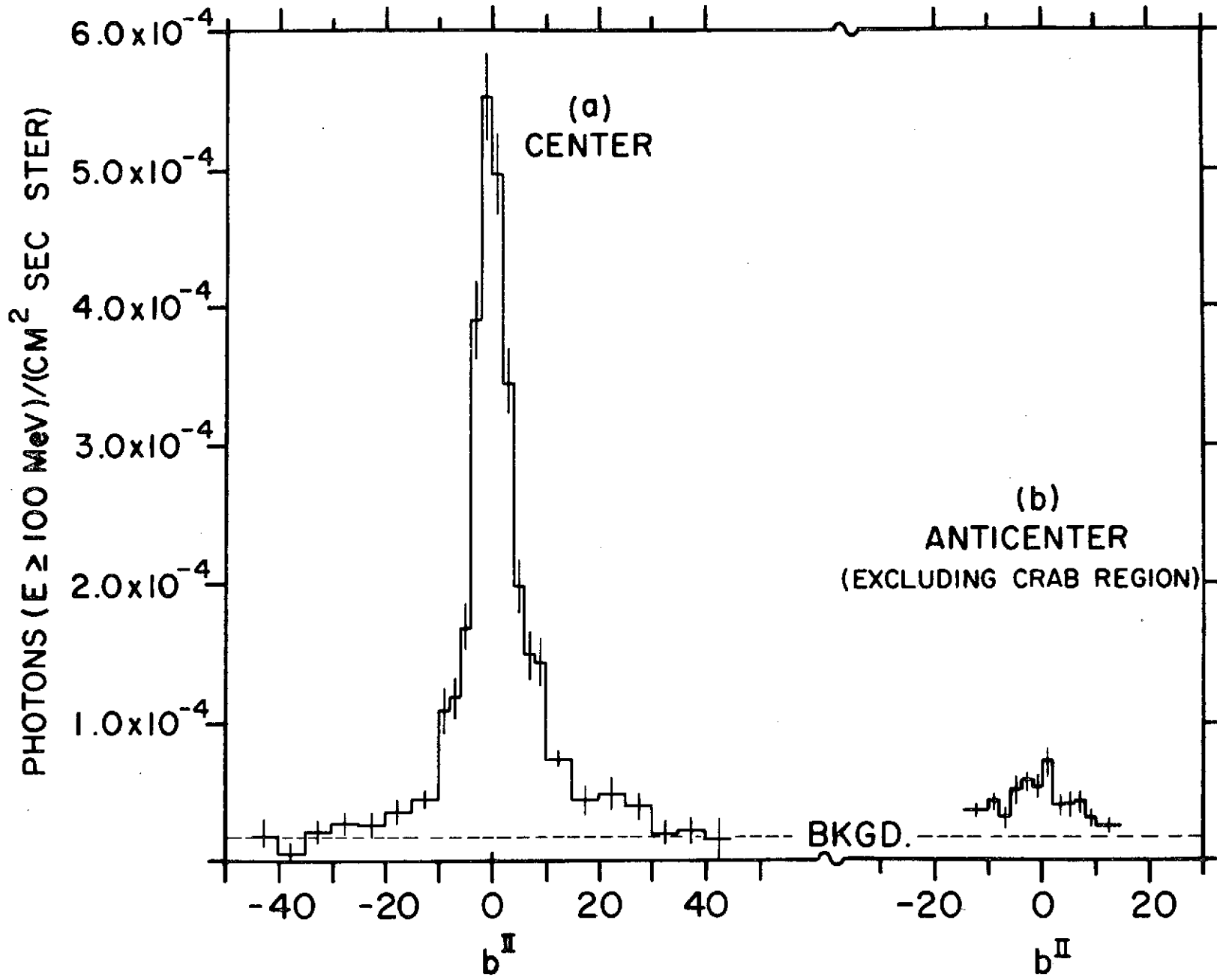
Fig. 9
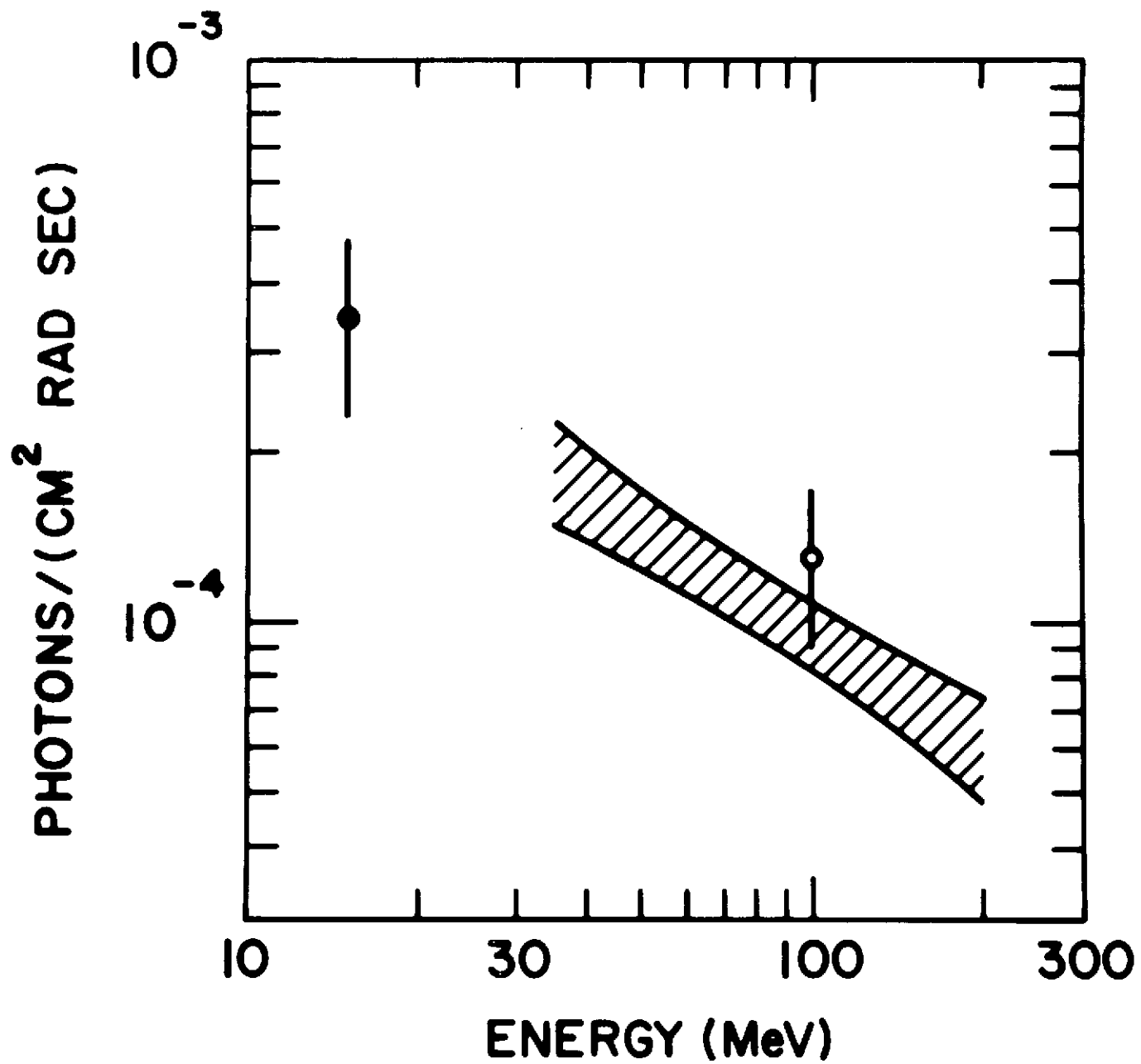
Fig. 10
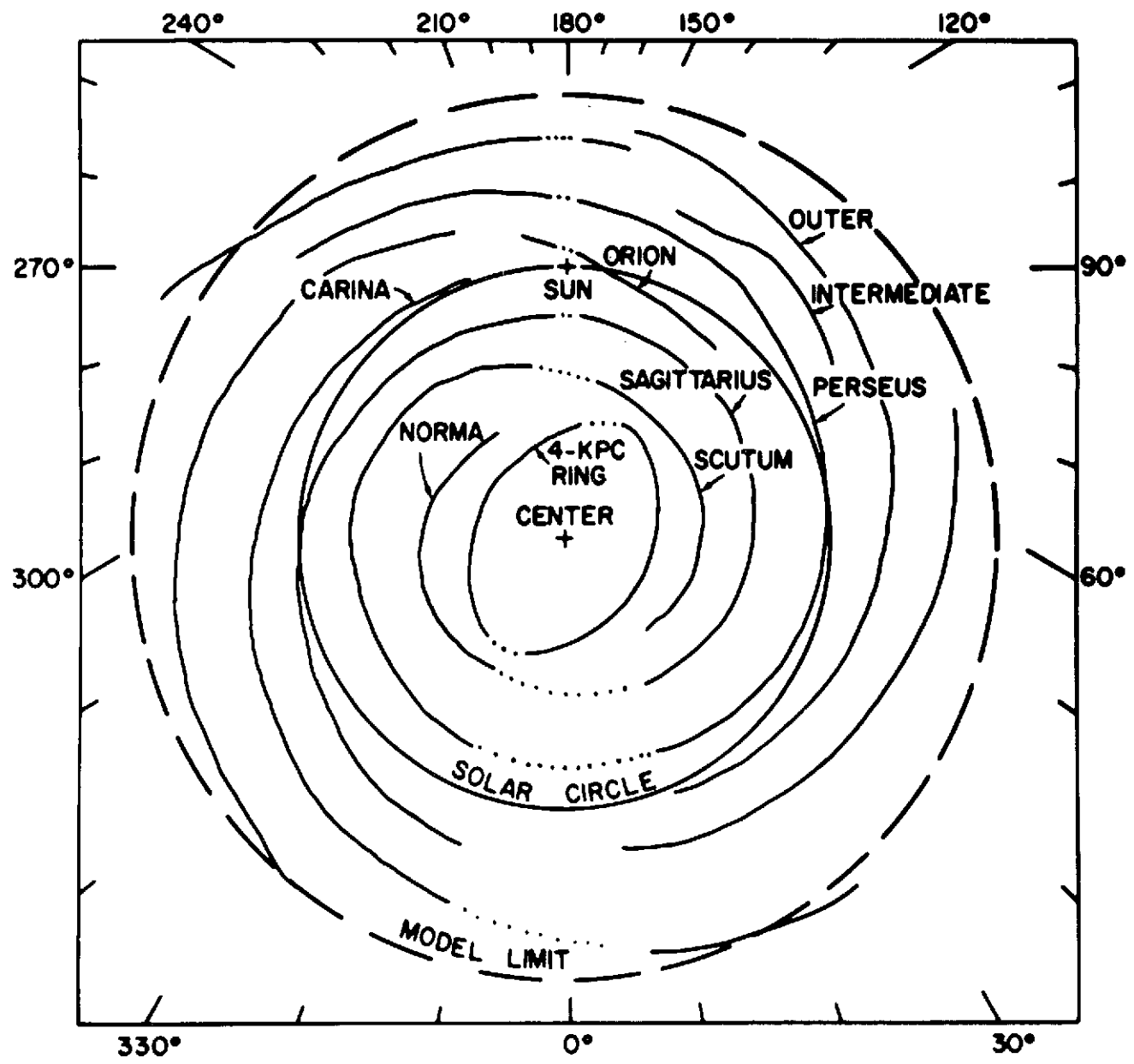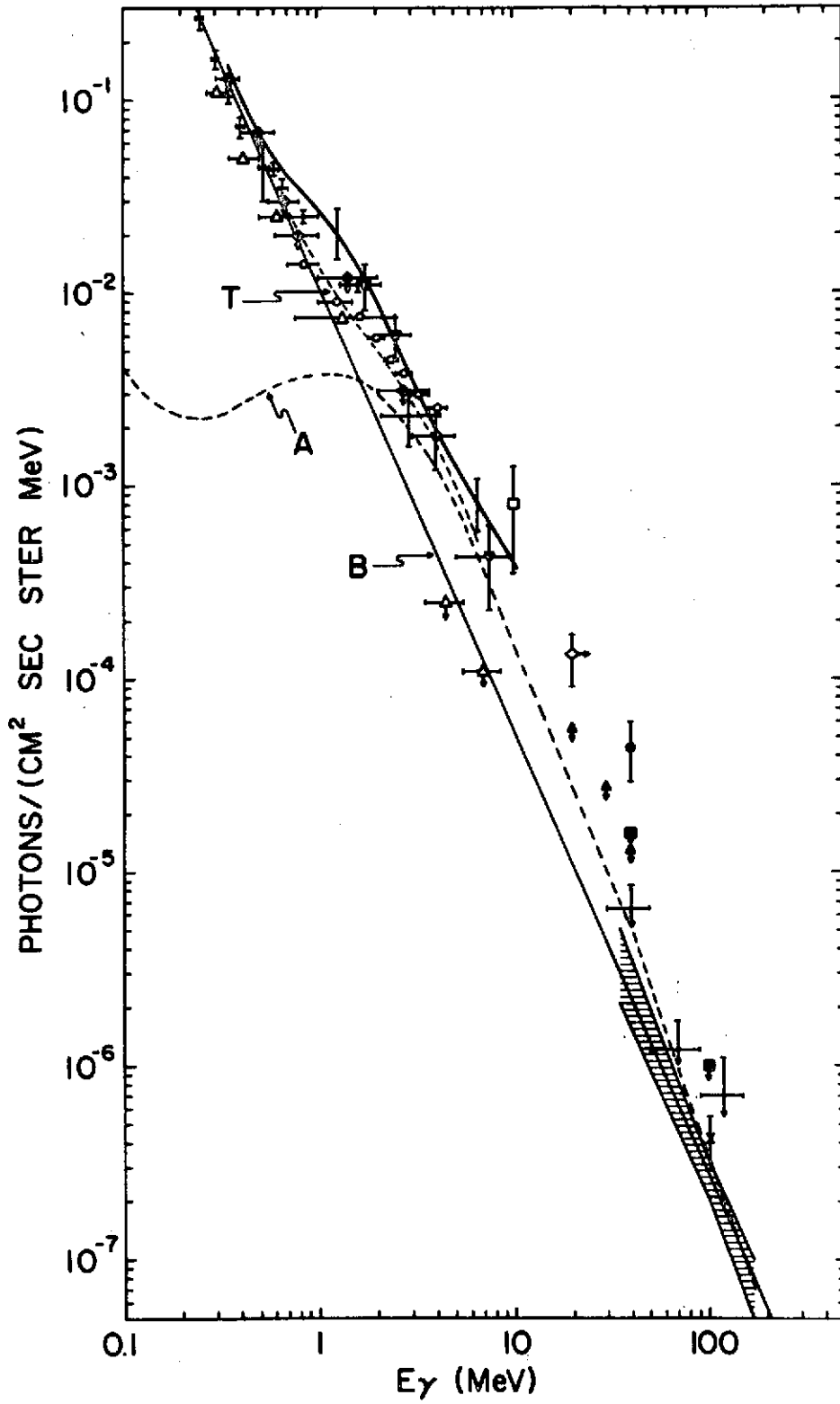
Fig. 11

Fig. 12

Fig. 13

Fig. A-1

Fig. A-2

NASA—GSFC